A refined output-only modal identification technique for structural health monitoring of civil infrastructures

Engineering Structures 323 (2025) 119210

Contents lists available at ScienceDirect

Engineering Structures

journal homepage: www.elsevier.com/locate/engstruct

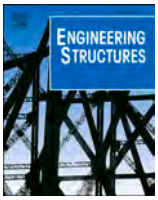

A refined output-only modal identification technique for structural health monitoring of civil infrastructures

Alessandro Cardoni *, Amir Reza Elahi, Gian Paolo Cimellaro

Dept. of Structural, Geotechnical, and Building Engineering, Politecnico di Torino, Corso Duca degli Abruzzi 24, 10129 Turin, Italy

ARTICLE INFO

Keywords:
Structural health monitoring
Operational modal analysis
Machine learning
Modal identification
Cable-stayed bridge
Footbridge
Cultural heritage

ABSTRACT

The increasing installation of structural health monitoring systems has raised the need for efficient and rapid data interpretation algorithms. Operational modal analysis is currently one of the most used techniques for extracting modal properties, and some attempts have been made to automate this procedure. However, automated techniques often require manual calibration of hyperparameters and show inconsistencies across different case studies. This paper proposes a refined version of the automated frequency domain decomposition (AFDD) using the modal assurance criterion (MAC) to obtain natural frequencies and mode shapes. Sensitivity analyses were conducted on the ambient vibration response of the Yonghe cable-stayed bridge in China, accounting for influential factors including noise levels, acceleration record length, sensor layouts. A novel approach is then introduced to interpret the results of the sensitivity analyses. The approach consists in plotting the result of each analysis in a stabilization diagram and then using a Gaussian mixture model that clusters the poles into core and outliers. This allows to identify regions where the MAC thresholds are optimal. By comparing the results of all the sensitivity analyses it was possible to define a single optimal MAC threshold, avoiding the need for fixing a value based on the user's experience. Three substantially different case studies were analyzed to extensively test the methodology: the Yonghe cable-stayed bridge, the PolyU footbridge in Hong Kong, and Moletta Tower in the Circus Maximus archeological site in Italy. The analysis compared the proposed AFDD algorithm to the traditional frequency domain decomposition and covariance-driven stochastic subspace identification. Specifically, the efficiency in identifying close frequencies, weakly excited modes, spurious peaks, and complex modes was evaluated for each method, which highlighted the robustness of the proposed optimized AFDD. The analysis showcases peculiar characteristics and drawbacks of each method when trying to identify complex vibrational modes of the specific case studies. It was found that the proposed AFDD procedure performs better than traditional methods despite it may misidentify complex modes due to the constraints of a narrower modal domain and similar geometries.

1. Introduction

Vibration-based structural health monitoring (SHM) has seen an increasing application in civil engineering to extract modal parameters, which can be used to better understand the dynamics of existing structural systems [1], calibrate and update numerical models [2–4], identify damage [5–7], avoid catastrophic collapses [8,9], and study seismic retrofit solutions [10].

One of the most commonly used approaches to identify modal properties is the operational modal analysis (OMA). Its popularity is mainly due to the fact that it does not require applying external excitation forces other than environmental vibrations nor measuring the actual exciting input. This is particularly convenient when monitoring building heritage, where achieving proper excitation levels through external forces is virtually impossible due to disproportionate costs and potential damage.

OMA techniques can be categorized into the time and frequency domains. In the time domain, stochastic subspace identification (SSI) [11] and auto regression moving average (ARMA) [12] have been widely applied. When applying the ARMA algorithm, it is necessary to estimate auto-regression and moving average coefficients using optimization tools. The algorithm might encounter convergence issues when estimating these parameters for complex structures or inputs with high levels of noise. Furthermore, real-time monitoring is almost impossible

* Corresponding author.
E-mail addresses: alessandro.cardoni@polito.it (A. Cardoni), amir.elahi@polito.it (A.R. Elahi), gianpaolo.cimellaro@polito.it (G.P. Cimellaro).

https://doi.org/10.1016/j.engstruct.2024.119210
Received 16 July 2024; Received in revised form 26 September 2024; Accepted 21 October 2024
Available online 3 November 2024

due to the high computational cost associated with its iterative optimization tool [13]. Conversely, the SSI exhibits superior performance overall, and for this reason it is often the preferred method. It has two primary branches denoted as covariance-driven SSI (cov-SSI) and data-driven SSI. The former relies on the correlation function derived from the input signal, while the latter processes the input directly. The SSI methodology involves estimating the model order, a challenging task in dynamically complex structures. Hence, an iterative approach is applied by assigning different model orders and constructing stabilization diagrams. In a stabilization diagram, physical and spurious poles are distinguished by setting appropriate thresholds. Stable modes are identified by combining judicious reasoning with experience, considering physical poles that form vertical alignments [14].

In the frequency domain, the fact that when a structure is subjected to ambient vibration it exhibits higher energy around its natural frequencies led to one of the first methods of OMA that is generally referred to as peak-picking [15]. This consists in plotting the power spectral density (PSD) spectrum computing the discrete Fourier transform, where the peaks represent the main frequencies of the structure. While this is a rapid frequency assessment tool, it can be effectively used only in case of clearly separated modes with low damping ratios. On the other hand, the frequency domain decomposition (FDD) is a more effective frequency domain technique that has been extensively used [16]. Derived from the general peak-picking method, the FDD rectifies its limitations by employing singular value decomposition (SVD) on the PSD. The modal properties obtained from FDD are limited to natural frequencies and mode shapes, while other versions of the method, such as the enhanced FDD, allow to estimate also damping ratios [17]. Overall, traditional techniques require the intervention of the user to select and interpret data. In some instances, this is not an easy task, even for experienced engineers. Furthermore, the effort required by traditional techniques for a real-time analysis of the ambient vibration response would be unreasonable. Therefore, many efforts have been directed toward automating OMA methods. The next section presents and discuss the main automated methods available in the literature for both time and frequency domains.

Despite the considerable research done in the automatic identification of modal parameters, the application of existing methods is often limited and might lead to inconsistent results. This study offers new practical insights in the application of an automated FDD (AFDD) procedure to reduce the bias of setting calibration parameters based on experience. Specifically, the AFDD procedure relies on the predefinition of a threshold for the modal assurance criterion (MAC). Depending on the type of SHM data and the characteristics of the structure, this may substantially vary. First, the effect of various variables related to the SHM system, i.e., noise level, record length, number of sensors, and sensor layout is investigated. Their effect on the performance of the AFDD is evaluated for various MAC thresholds through a series of sensitivity analyses using real data from the Yonghe cable-stayed bridge in China. This benchmark was selected since there is a lack of comprehensive studies on damage identification and monitoring of cable-stayed bridges based on experimental data [18]. Then, a Gaussian mixture model (GMM), an algorithm belonging to the category of unsupervised machine learning (ML), was implemented to process the results obtained from the sensitivity analyses and cluster them into core poles and outliers. As a result, the optimal ranges of MAC were estimated for each variable and a common optimal threshold was identified. This novel approach can be easily replicated by engineers and researchers who would like to establish an unbiased MAC threshold that optimize results depending on the characteristics of structure and SHM system. Nonetheless, the optimal value resulting from the sensitivity analyses on the the Yonghe bridge could already be valid in several applications, potentially removing the need for further fine-tuning. To verify this, an in-depth test was carried out on significantly different structures using the previously determined threshold. The performance was compared to the traditional FDD and cov-SSI. The first case study is the Yonghe cable-stayed bridge, which was tested using acceleration records different from those used to determine the optimal MAC threshold. The second case study is the PolyU footbridge on the Main Campus of the Hong Kong Polytechnic University. Footbridges are typically characterized by their complex dynamics. Excessive vibration of the Millennium Bridge in London, Changi Mezzanine in Singapore, Toda Park Bridge in Japan, and the collapse of the Vltava River bridge in Prague highlight the lack of monitoring and SHM studies on them [19]. The third application concerns the Moletta tower, a cultural heritage structure part of the Circus Maximus archeological site in Rome, Italy. Its exposure to various sources of excitations and the fact that it is partially buried under alluvial soil due to flooding events, make its dynamic characterization challenging [20].

Results show that the proposed AFDD method outperforms the traditional OMA procedures in estimating modal properties. However, an SHM system with proper spatial resolution should be designed when dealing with structures characterized by complex dynamics. This ensures a better distinction of modal properties since the proposed method is based on the geometry of mode shapes.

The paper is organized as follows. Section 2 discusses the main automated OMA procedures available in the literature. Section 3 outlines a brief mathematical background of the GMM algorithm chosen to determine the optimal MAC threshold, the OMA techniques used in this study, and the proposed methodology. The results of the sensitivity analyses of factors affecting modal estimations are presented in Section 4. In Section 5, the AFDD with optimal MAC threshold is tested on the three case studies, and the results are compared with traditional FDD and cov-SSI methodologies. Finally, the concluding remarks and limitations of the proposed procedure are presented in Section 6.

2. Existing automated OMA procedures

The main challenge in automating the SSI procedure is the interpretation of the stabilization diagram, since the distinction between physical and non-physical modes is not always obvious. To tackle this issue, Li et al. developed a time-discrete state-space model that connects the second order blind identification (SOBI) and cov-SSI algorithms [21]. The methodology identifies the model order directly by SOBI and exploits the cov-SSI afterward to avoid building stabilization diagrams. In addition, the source signals are analyzed to help selecting physical modes. The physical modal responses obtained from SOBI exhibit sinusoidal decay in the time domain and a spectral peak in the frequency domain. Despite its reduced reliance on expert intervention, the procedure cannot be considered fully automated.

Existing automated procedures in the time domain mainly rely on ML algorithms for segmenting and clustering the poles of the stabilization diagrams [14,22]. In a seminal study by Magalhaes et al. [23], the cov-SSI procedure was automated using a hierarchical clustering algorithm to analyze poles within the stabilization diagram. Clusters with a certain number of points were identified as physical modes, while others were regarded as spurious and discarded based on a predefined cutoff threshold. A robust approach to estimate the cutoff threshold was implemented by Zini et al. [24], who analyzed the distribution of the distance between poles related to consecutive model orders and then suggested to take the 80th percentile value as cutoff. However, methodologies based on statistical analysis could present some drawbacks when identifying closely spaced dynamic modes. To overcome the limitation of having to set the number of clusters a priori, Romanazzi et al. proposed an iterative procedure for hierarchical clustering that has the advantage of inferring the number of clusters [25]. Despite the procedure is sensitive to the weighting coefficient used to estimate the distance between poles, the simulations and experimental validation demonstrated stability and robustness. In another SSI automation attempt by Rosso et. al [26], a procedure was developed to analyze the stabilization diagram through kernel density estimation instead of traditional clustering techniques. The method involves a nonparametric

estimation of probability density functions from the physical poles in the stabilization diagram and the hyperparameters are handled through Maximum Likelihood and Sheather–Jones algorithms which result in a significant computational effort.

In another work, Ye et al. [27] introduced innovative stabilization diagrams derived from combining NExT/ERA [28] procedures and hierarchical clustering analysis. The stabilization diagram was built from filtered modes, and hierarchical clustering was applied to automate the analysis. During the clustering process, the Tau test was also utilized to exclude data with discrete damping ratios denoted as outliers. Nonetheless, the procedure necessitates expert supervision due to the significant number of parameters that need to be set in advance.

Furthermore, the identification of modes corresponding to close frequencies, lightly excited modes, and generalization for different structural systems is still an open issue. The work conducted by Dederichs et al. [29] highlighted the limitations in the performance of automated time domain approaches using clustering algorithms. It demonstrated the ability of six techniques to extract modal properties automatically from the Hardanger suspension bridge in Norway. Their performance was evaluated in terms of mode detection rate, false mode detections, and duplicate modal detections. The detection rate derived for these methodologies spanned from 39.8 % to 81.2 %, demonstrating variable reliability depending on the chosen method. Time domain approaches also show limitations in extracting modal properties of systems under narrowband excitation. For instance, the study conducted by Sun et al. [30] discloses the challenge in distinction between harmonic action produced by bell and natural frequencies of the system.

In the frequency domain, in a study by Kim et al. [31], the automation consists in detecting peak regions in the SV spectrum using a Faster R-CNN convolutional neural network and subsequent post-processing to identify vibration modes. The network was trained by generated numerical models related to an MDOF system. It outperformed the automated SSI described by Magalhães et al. [23] in the modal identification of various case studies, achieving an F1 score of 0.92 with less computational effort. Yet, the main limitation of the neural network lies in the distinction of closely spaced modes with high damping and points located at the boundaries of the peak regions in the SV spectrum. In another study by Jeong et al. [32], a deep learning network was trained and validated for automatic peak picking in the SV spectrum to estimate the tension force of bridge cables. The study revealed the robustness of automated methods in the frequency domain, suitable for application in various fields of SHM. The benefit of using ML algorithms is their independence from frequency range selection or fixing predefined thresholds. However, they are highly affected by the training data set and their hyperparameter tuning. Consequently, the use of ML algorithms for automating FDD needs further research.

The AFDD methodology, based on the geometry of mode shapes, was proposed by Brincker et al. [33] to identify closely spaced modes and reduce the expert intervention. It was based on identifying a domain around an SV peak using a modal domain and coherence function. Magalhães et al.[34] further adopted this technique using the MAC, which successfully distinguished physical and non-physical modes in the monitoring of the Infante D. Henrique Bridge in Portugal. In that study, the MAC threshold was fixed at 0.4 by experience, and it was recommended to perform a preliminary analysis to establish the appropriate thresholds, accounting for various factors influencing modal characteristics. While using AFDD with MAC has proven to be effective, several factors can influence its accuracy and there are significant limitations. For instance, previous studies struggled in identifying frequencies that are close to each other and complex dynamic modes. Additionally, when analyzing structures with different characteristics, one may need to subjectively define a different threshold for each case.

3. Methodology

3.1. Gaussian Mixture Model (GMM)

The Gaussian mixture model (GMM) is an unsupervised ML technique used for clustering. It models complex data sets into separate clusters by combining multiple normal distributions named Gaussian components. In addition, by modeling the normal behavior of datasets, any data point deviating significantly from the learned distribution can be identified as an anomaly. A GMM for a data point present in the vector $\mathbf{x}$ with the dimension of D is defined by a weighted sum of K Gaussian components expressed as:

$$p(\mathbf{x}) = \sum_{k=1}^{K} \pi_k \cdot \Omega(\mathbf{x}_n | \boldsymbol{\mu}_k, \boldsymbol{\Sigma}_k) \tag{1}$$

where Ω represents the Gaussian distribution, and each Gaussian component is characterized by its mean ($\boldsymbol{\mu}_k$), covariance matrix ($\boldsymbol{\Sigma}_k$), and mixing coefficient ($\boldsymbol{\pi}_k$) [35,36]. To estimate the parameters of the Gaussian components that best describe the input dataset, the maximum likelihood estimation is exploited. The likelihood function is defined as the product of the probability density functions of the individual Gaussian components, each weighted by its mixing coefficient. Its logarithmic form for the input matrix of $\mathbf{X} = \{\mathbf{x}_1, \mathbf{x}_2, ..., \mathbf{x}_N\}$ is:

$$\ln p\left(\mathbf{X} | \boldsymbol{\pi}, \boldsymbol{\mu}, \boldsymbol{\Sigma}\right) = \sum_{n=1}^{N} \ln \left\{ \sum_{k=1}^{K} \pi_k \cdot \Omega(\mathbf{x}_n | \boldsymbol{\mu}_k, \boldsymbol{\Sigma}_k) \right\} \tag{2}$$

Expectation-Maximization is a robust algorithm to maximize this likelihood solution, which determines $\boldsymbol{\mu}_k$, $\boldsymbol{\Sigma}_k$, $\boldsymbol{\pi}_k$ iteratively [37]. As the name suggests, it consists of two main steps, expectation (E) and maximization (M). In the E-step, the posterior probability ($\gamma(z_{nk})$), i.e., the probability of data point x_n belonging to Gaussian component k, is computed as shown in Eq. (3).

$$\gamma(z_{nk}) = \frac{\pi_k \Omega(\mathbf{x}_n | \boldsymbol{\mu}_k, \boldsymbol{\Sigma}_k)}{\sum_{j=1}^{K} \pi_j \Omega\left(\mathbf{x}_n | \boldsymbol{\mu}_j, \boldsymbol{\Sigma}_j\right)} \tag{3}$$

In the M-step, GMM parameters are updated using the posterior probabilities calculated in the E-step:

$$\boldsymbol{\mu}_k^{new} = \frac{1}{N_k} \sum_{n=1}^{N} \gamma(z_{nk}) \mathbf{x}_n \tag{4}$$

$$\boldsymbol{\Sigma}_k^{new} = \frac{1}{N_k} \sum_{n=1}^{N} \gamma(z_{nk}) \left(\mathbf{x}_n - \boldsymbol{\mu}_k^{new}\right) \left(\mathbf{x}_n - \boldsymbol{\mu}_k^{new}\right)^T \tag{5}$$

$$\pi_k^{new} = \frac{N_k}{N} \tag{6}$$

$$N_k = \sum_{n=1}^{N} \gamma(z_{nk}) \tag{7}$$

In Eqs. (4–7), N is the total number of data points, N_K is the sum of posterior probabilities for component k, and z_{nk} represents the latent variable, indicating the GMM component assignment for data point x_n. Once the new parameters are obtained, they are used in the likelihood function to check its convergence.

3.2. Covariance-driven stochastic subspace identification (cov-SSI)

The SSI technique exploits a state-space model to reformulate a second-order partial differential equation in terms of two separate first-order state and observation problems. Through the cov-SSI identification, the following discrete-time state space model is proposed, where the input is assumed to be a white noise signal. Eq. (8) describes the

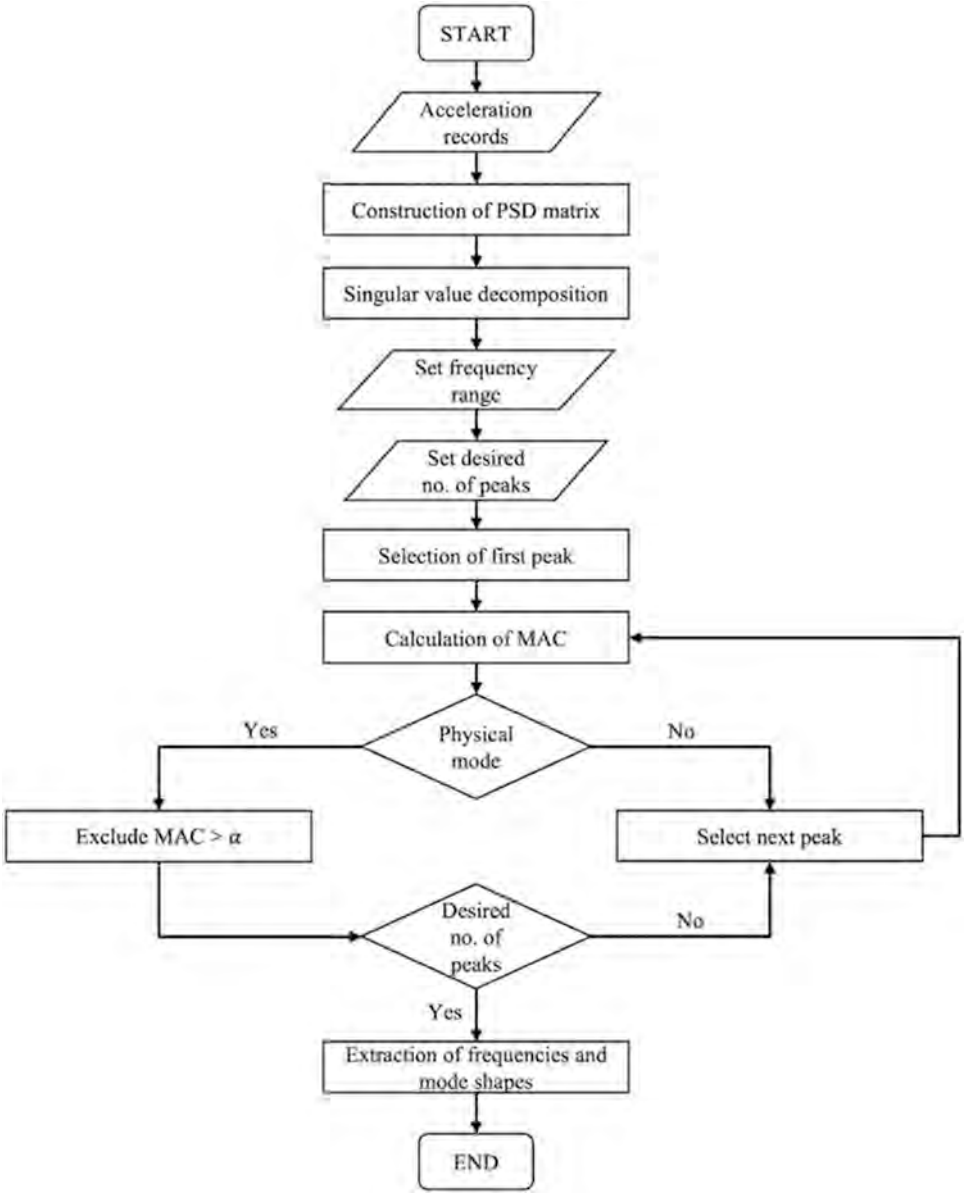

Fig. 1. Flowchart of the AFDD algorithm.

model, where $\mathbf{x}_k$ and $\mathbf{y}_k$ are the state and recorded output vectors at time instant k, respectively.

$$\begin{aligned}\mathbf{x}_{k+1} &= \mathbf{A}\cdot\mathbf{x}_k + \mathbf{w}_k \\ \mathbf{y}_k &= \mathbf{C}\cdot\mathbf{x}_k + \mathbf{v}_k\end{aligned} \tag{8}$$

The discrete state and output matrices are **A** and **C**, where the modal properties are extracted from. The vector $\mathbf{w}_k$ represents the model inaccuracy, while $\mathbf{v}_k$ describes the sensor measurement bias. The analysis begins by estimating the output covariance ($\mathbf{R}_i$) from the correlation between ambient vibration responses as shown in Eq. (9):

$$\mathbf{R}_i = \frac{1}{N-i}\sum_{k=1}^{N-i-1}\mathbf{y}_{k+i}\cdot\mathbf{y}_k^T \tag{9}$$

where N is the length of the discrete output, i is the time lag parameter, and $\mathbf{y}_k^T$ is the output's transpose. The Toeplitz matrix $\mathbf{T}_{1|i}$ is then computed from the output covariance ($\mathbf{R}_i$) as indicated in Eq. (10).

$$\mathbf{T}_{1|i} = \begin{bmatrix} \mathbf{R}_i & \mathbf{R}_{i-1} & \cdots & \mathbf{R}_1 \\ \mathbf{R}_{i+1} & \mathbf{R}_i & \cdots & \mathbf{R}_2 \\ \vdots & \vdots & \ddots & \vdots \\ \mathbf{R}_{2i-1} & \mathbf{R}_{2i-2} & \cdots & \mathbf{R}_i \end{bmatrix} \tag{10}$$

The cov-SSI is a stochastic realization problem aiming at building an observable and controllable model [11]. To build the model, for a system with order n, it is necessary to obtain the observability matrix **O** and the controllability matrix **Γ** with rank equal to n. Matrices **O** and **Γ** are estimated from the singular value decomposition (SVD) of the Toeplitz matrix:

$$\begin{aligned}\mathbf{T}_{1|i} &= \mathbf{O}_i\mathbf{\Gamma}_i = \mathbf{U}_1\mathbf{\Sigma}_1\mathbf{V}_1^T \\ \mathbf{O}_i &= \mathbf{U}_1\mathbf{\Sigma}_1^{1/2}\mathbf{M} \\ \mathbf{\Gamma}_i &= \mathbf{M}^{-1}\mathbf{\Sigma}_1^{1/2}\mathbf{V}_1^T\end{aligned} \tag{11}$$

In Eq. (11) $\mathbf{U}_1$ and $\mathbf{V}_1$ are orthogonal matrices consisting of singular vectors, $\mathbf{\Sigma}_1$ contains the singular values arranged in ascending order, and **M** is assumed to be an identity matrix. After determining matrices **O** and **Γ**, many algorithms can be used to determine the discrete state and

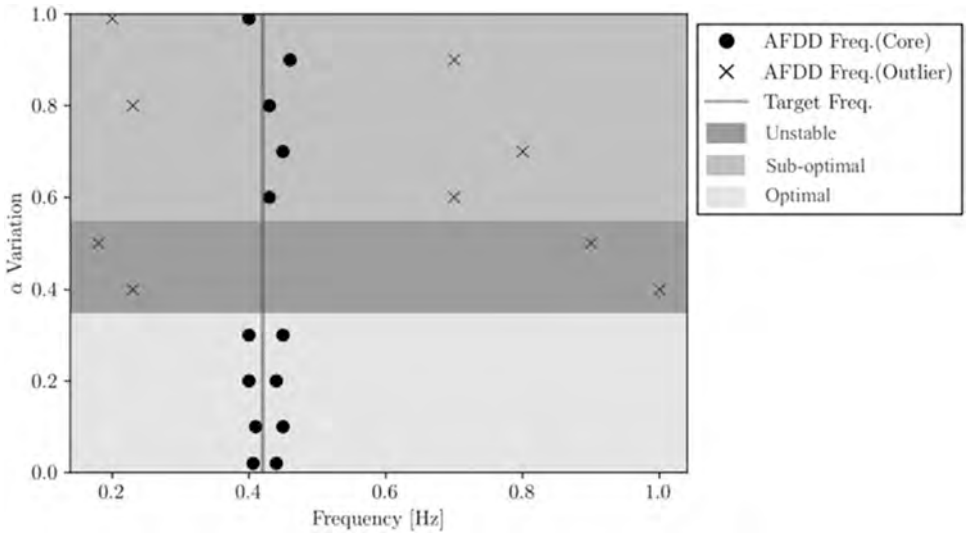

Fig. 2. Interpretation of a stabilization diagram through a GMM.

output matrices (**A** and **C**) [38]. Once the components of the state space model are determined, the natural frequencies and mode shapes are obtained by performing Eigen value decomposition.

In the cov-SSI analysis, two main parameters should be defined. The first parameter is the time lag. This can be chosen by analyzing the PSD diagram and identifying the system's fundamental frequency [39]. Based on the sampling frequency (f_s) and fundamental frequency (f_f), the time lag i is defined as shown by Eq. (12).

$$i = 1.5\frac{f_s}{f_f} \tag{12}$$

The second parameter is the order of the model. This parameter cannot be univocally quantified. Typically, a value within the range of 4 to 30 times the desired number of mode shapes is suggested [40].

Finally, to identify stable poles it is necessary to define limitations on frequency, damping ratio, and mode shape. In this research, the limitations suggested by Lee et al. [41] are adopted. They have been used by several researchers and compared to other values that can be found in the literature they are stricter, which enhances the accuracy of the stabilization diagrams. These limitations are reported in Eq. (13):

$$\begin{aligned}
&\text{Frequency}: \ \frac{\left|f^{(p+1)} + f^{(p)}\right|}{f^{(p)}} \times 100\% < 1\% \\
&\text{Dampingratio}: \ \frac{\left|\xi^{(p+1)} + \xi^{(p)}\right|}{\xi^{(p)}} \times 100\% < 5\% \\
&\text{Modeshape}: \ \left(1 - \text{MAC}\left(\boldsymbol{\phi}^{p}, \boldsymbol{\phi}^{p+1}\right)\right) \times 100\% < 3\%
\end{aligned} \tag{13}$$

where f,ξ and $\boldsymbol{\phi}$ are the natural frequencies, damping ratios, and mode shapes, respectively. The parameter p denotes the system order, and MAC is the modal assurance criterion between the mode shapes. The MAC of two vectors ($\mathbf{a}$, $\mathbf{b}$) can be calculated as shown in Eq. (14).

$$\text{MAC}\left(\mathbf{a}, \mathbf{b}\right) = \frac{|\mathbf{a}^T\mathbf{b}|^2}{(\mathbf{a}^T\mathbf{a})(\mathbf{b}^T\mathbf{b})} \tag{14}$$

In the current study, a MATLAB script was written to perform the cov-SSI analysis based on the procedure described by Otto [42].

3.3. Proposed automated frequency domain decomposition (AFDD) algorithm

In the FDD technique, the first step is to analyze the power distribution in the frequency domain by estimating the PSD matrix. This is derived from the Fourier transform of auto and cross-correlations. After some mathematical manipulation, the PSD of the output can be written at discrete frequencies ($i\omega$) as shown in Eq. (15):

$$\mathbf{G}_{yy}\left(i\omega\right) = \sum_{k \in sub(\omega)} \left(\frac{d_k \boldsymbol{\phi}_k \boldsymbol{\phi}_k^T}{i\omega - \boldsymbol{\lambda}_k} + \frac{d_k^* \boldsymbol{\phi}_k^* \boldsymbol{\phi}_k^H}{i\omega - \boldsymbol{\lambda}_k^*}\right) \tag{15}$$

where d is a scalar value obtained from the Fourier transform of the Dirac's function, $\boldsymbol{\phi}$ is the mode shape vector, and $\boldsymbol{\phi}_k^H$ is the complex conjugate of its transpose. $\boldsymbol{\lambda}_k$, $\boldsymbol{\lambda}_k^*$ denote the poles of modes n and its conjugate, respectively. Poles indicate complex numbers that are part of the transfer function's denominator. In the output PSD, each peak, a point with high energy, represents the dominance of a mode or its combination with those in proximity. The singular value decomposition (SVD) technique is typically used to obtain the modal properties near the peak. Being $\mathbf{G}_{yy}$ the PSD at discrete frequencies, its SVD is calculated as per Eq. (16):

$$\mathbf{G}_{yy}(i\omega) = \mathbf{U}_i \mathbf{S}_i \mathbf{V}_i^H \tag{16}$$

In this relation, **S** is a diagonal matrix formed by singular values in descending order. **U** and **V** are matrixes built from the corresponding first singular vectors [16]. From the resultant SV spectrum, it is possible to identify peaks representing the modes of vibrations.

Fig. 1 shows a flowchart that summarizes the proposed AFDD procedure. After processing the acceleration records via PSD and SVD, the user defines a certain frequency range and the number of modes that they would like to get. From this point, the algorithm selects the point with the largest SV value as the first peak. Then it calculates the MAC between the first peak mode shape and all the other mode shapes within the frequency range. To verify that the selected peak corresponds to a physical mode, a modal domain assessment is carried out, checking that the average MAC between the selected peak and neighbor points is 0.6 or higher, as suggested by Magalhães et al. [34]. If this condition is not satisfied, the second largest point should be selected as peak and the verification repeated. Then, to select other peaks representative of valid modes, a MAC threshold (α) should be defined. This ensures that SV points with similar mode shapes can be excluded. Assuming the α threshold is known, the SV points with a MAC value above the threshold are excluded from the selection of the next peak. Among the remaining points, the next possible peak is always the one with the largest value, provided that is a physical mode. The process is iterated until the desired number of peaks is matched and the frequencies and mode shapes can be extracted. However, the process might end before if there are no more

Table 1
Description of the algorithm used to define the optimal α values.

Algorithm 1: GMM-based sensitivity analysis using AFDD

1: **Procedure:** Identify the optimal value of MAC threshold (α)

2: **Input:** Target frequencies from FE model

3: V: Variables selected for the sensitivity analysis

4: N: Scenarios defined for each variable V

5: Acc: Acceleration record for each N

6: K: MAC threshold variation (α) → 0:0.2:1

7: **for** i =1:N

8: **for** α=(0:0.02:1)

9: **do** the AFDD analysis using Acc

10: **return** AFDD results

11: **end**

12: Generate a stabilization diagram with AFDD results and target frequencies

13: Cluster the AFDD results using the GMM

14: Analyze the number of AFDD frequencies in the outlier cluster for each α

15: Classify the α→ optimal, suboptimal, unstable

16: **end**

17: **Output:** Range of optimal MAC thresholds (α)

19: **end procedure**

points in the SV diagram to be selected as peaks. This could happen if the user selects a number of peaks that exceed the dynamic range of the structure or if the modes are too similar according to the chosen α threshold. Compared to the traditional FDD, where typically the user selects only the most prominent peaks (i.e., those with large amplitudes in the SV spectrum), this procedure allows to identify relevant mode shapes even when frequencies show lower amplitudes in the SV spectrum.

To avoid pre-defining the α threshold based on user's experience, it is proposed to carry out sensitivity analyses involving multiple variables on a benchmark with known modal properties to use as targets. For each variable, different relevant scenarios can be imagined. For instance, if the variable is the length of the acceleration records, one can investigate the effect of having 10-minute long vs. 1-hour long records. In each scenario, the AFDD analysis is performed varying the α threshold from 0 to 1, obtaining the desired frequencies and mode shapes that the method is able to determine under those premises. The results of each AFDD analysis are used to generate a stabilization diagram where it is

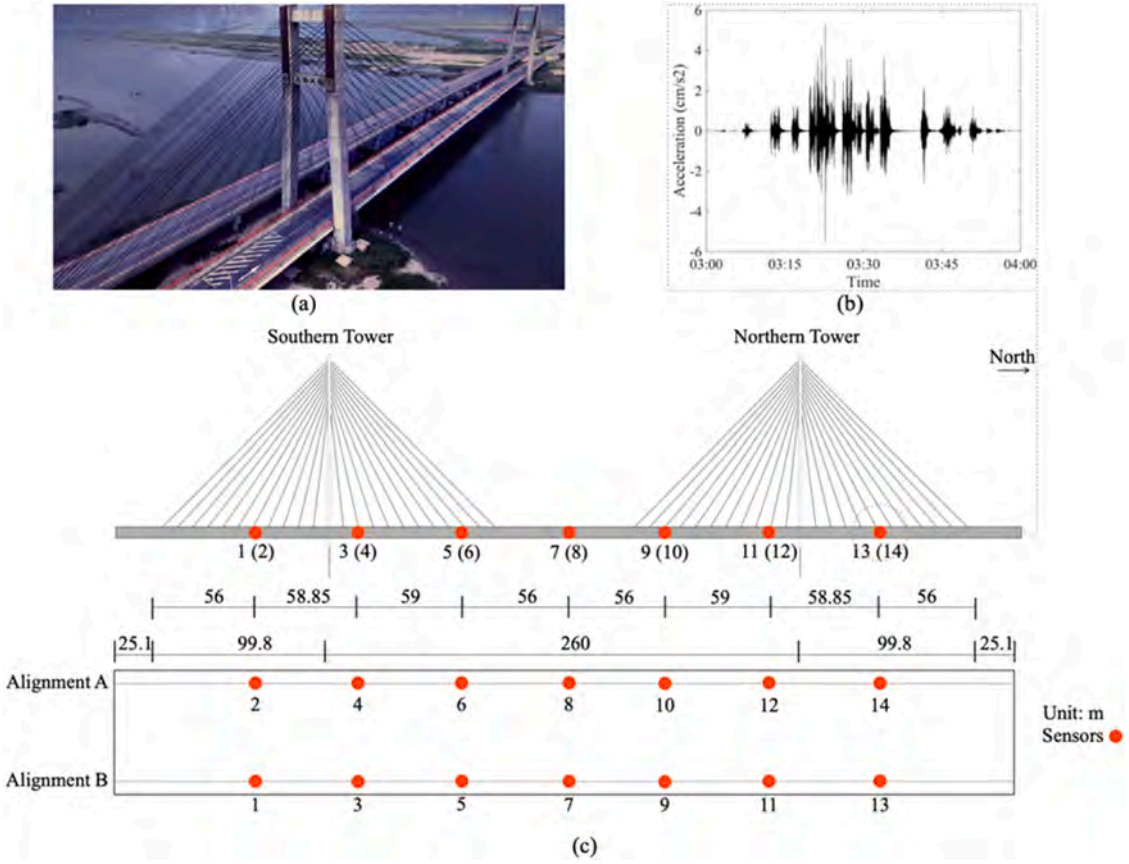

Fig. 3. (a) Yonghe cable-stayed bridge, (b) ambient vibration response recorded by sensor 14, (c) sensor layout.

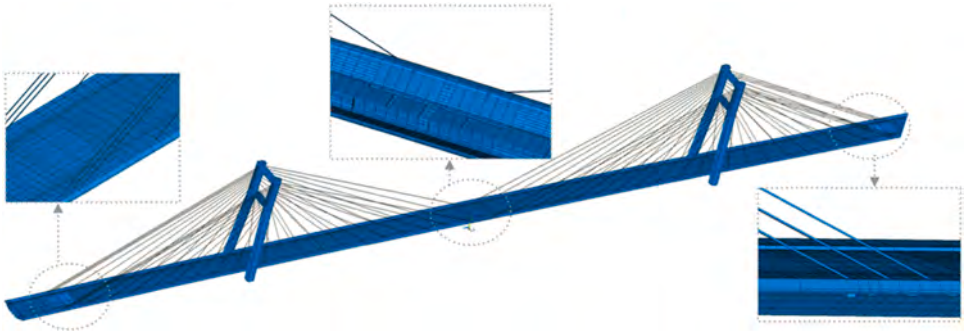

Fig. 4. FE model of Yonghe cable-stayed bridge.

possible to visualize the results corresponding to each α value. The stabilization diagram is interpreted through a GMM that clusters the results into core poles and outliers. The output of the GMM is illustrated with an example in Fig. 2 that simulates a possible outcome of a sensitivity analysis. The vertical line represents the target frequency, which could be known from a finite element (FE) model, while the scatter points denote simulated AFDD results. These are classified into core poles and outliers based on the distance to the target frequency. Points exceeding a 0.1 Hz distance are included in the outlier cluster. In addition, the output of GMM allows to define optimal, suboptimal, and unstable regions in the diagram, meaning that different ranges of α values lead to different accuracy of the results. It is considered that if for a fixed α all the AFDD estimates fall inside the core cluster, then the α is optimal. On the other hand, if the selected α leads to having one pole in the outlier cluster, then it is regarded as suboptimal. Finally, the unstable region includes all α values leading to two or more outliers. This entire procedure is summarized by the algorithm in Table 1. Once the unstable, sub-optimal, and optimal regions are defined for each scenario of all considered variables, it is possible to select an α threshold that consistently fits within the optimal regions.

A MATLAB script was developed based on the above formulation and the procedures described in [33] and[34]. The extracted modal properties are limited to the natural frequencies and mode shapes.

4. Optimization of the AFDD

Although the AFDD methodology has proven to be effective in several research works, there are still some factors that can greatly affect the accuracy of the results. In this section, a series of sensitivity analyses is performed to evaluate the influence of different factors and establish when the optimal performance is achieved. The analyses were carried out using the experimental data from the Yonghe cable-stayed bridge to

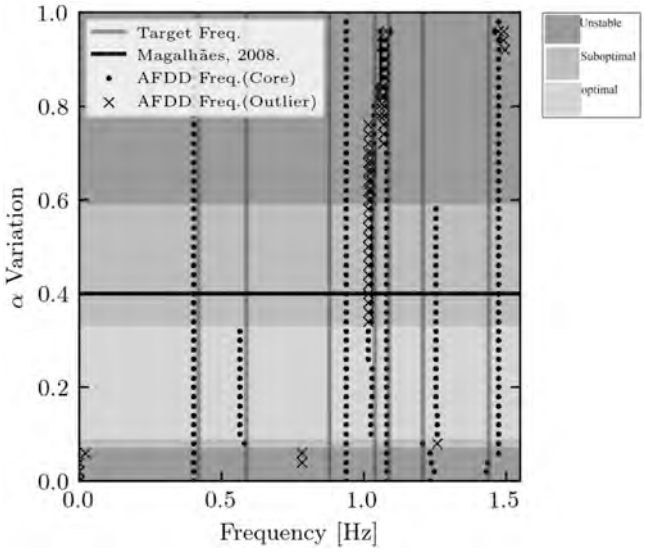

Fig. 5. The effect of α variation on the AFDD outcomes.

acquire AFDD's optimal performance.

4.1. Description of the benchmark for the sensitivity analyses

The Yonghe cable-stayed bridge is located in the port of Tianjin, Hebei Province, China. The total length of the bridge is 510 m, and the deck width is 11 m. It consists of a 210 m main span and two 125 m secondary spans. The deck is connected to the north and south towers by 88 pairs of 5 mm cables. During retrofit interventions in 2005–2007, the infrastructure was instrumented with an innovative SHM system that included more than 150 sensors, 14 of which being uniaxial accelerometers mounted on the deck [43], as illustrated in Fig. 3.

Li et al. [43] developed an FE model in ANSYS Mechanical APDL [44] and they kindly provided it to us. The main girders and towers were modeled using the three-dimensional beam element (BEAM 44), while the mass elements and linear elastic links (LINK 10) were assigned to the transverse beams and cables, respectively. All boundary conditions were defined accordingly, including the rubber supports (Fig. 4). The model had already been calibrated through a long-term monitoring campaign. Therefore, it was possible to perform the modal analysis directly on ANSYS model, obtaining the target frequencies for vertical modes, i.e., the relevant direction since the sensors measured only the vertical accelerations. At the same time, the modal coordinates of the middle longitudinal axis were extracted from the software. Specifically, the ones aligned with the sensor grid were considered to compare the mode shapes obtained from AFDD and cov-SSI analyses.

The records considered through all the sensitivity analyses, unless otherwise stated, are the actual ambient vibrations recorded from 8:00 p.m. to 12:00 a.m. of January 17, 2008.

4.2. Preprocessing of acceleration records

The raw acceleration time histories were preprocessed with Hunning window filtering to remove spikes and irregular trends. Additionally, the records were filtered through a six-order Butterworth bandpass with low and high-frequency cuts of 0.1 Hz and 30 Hz [45]. A baseline correction was then performed using OpenSeismosignal [46].

Depending on the type of sensors used, the recorded signals of ambient vibrations might exhibit significant noise. To reduce the noise, a method based on the SVD was exploited, where a matrix of rank r comprised of the noisy signals is truncated, assuming the presence of singular values equal to zero, as shown in Eq. (17).

$$\mathbf{Y} = [\mathbf{U}_r, \mathbf{U}_{m-r}] \begin{bmatrix} \mathbf{S}_r & 0 \\ 0 & 0 \end{bmatrix} \begin{bmatrix} \mathbf{V}_r^T \\ \mathbf{U}_{n-r}^T \end{bmatrix} = \mathbf{U}_r \mathbf{S}_r \mathbf{V}_r^T \tag{17}$$

In this formula $\mathbf{U}_r$ and $\mathbf{V}_r$ are orthogonal matrices related to singular vectors, and $\mathbf{S}_r$ is its corresponding matrix with singular values in the principal diagonal. The methodology consists of the following steps:

Step 1. Generating a Hankel matrix $\mathbf{Y}$ with dimensions (m,n) from the signal $\mathbf{y}$:

$$\mathbf{Y}_{m,n} = \begin{bmatrix} y_1 & y_2 & \dots & y_n \\ y_2 & y_3 & \dots & y_{n+1} \\ \vdots & \vdots & \ddots & \vdots \\ y_m & y_{m+1} & \dots & y_N \end{bmatrix} \tag{18}$$

Step 2. Dividing the Hankel matrix into a healthy $(\mathbf{X}_{m,n})$ and a noisy subspace$(\mathbf{N}_{m,n})$:

$$\mathbf{Y}_{m,n} = \mathbf{X}_{m,n} + \mathbf{N}_{m,n} \tag{19}$$

Step 3. Reducing the noise by decomposing the structured Hankel matrix $\mathbf{Y}$ using the SVD combined with subsequence truncation of small SVs:

$$\mathbf{Y}_{m,n} = \sum_{i=1}^{m} s_i \mathbf{u}_i \mathbf{v}_i^T = \sum_{i=1}^{l} s_i \mathbf{u}_i \mathbf{v}_i^T + \sum_{i=l+1}^{m} s_i \mathbf{u}_i \mathbf{v}_i^T = \mathbf{X}_{m,n} + \mathbf{N}_{m,n} \tag{20}$$

$$s_1 > s_2 > \dots > s_l \gg s_{l+1} = s_{l+2} = \dots = s_m \approx 0$$

where $s_i, \mathbf{u}_i, \mathbf{v}_i^T$ are the SVs and corresponding singular vectors, while l and m are two calibration parameters.

Step 4. Generating the de-noised signal vector with $\overline{x}_i$ elements from the non-Hankel de-noised matrix using arithmetic averaging of anti-diagonal elements [47]:

$$\mathbf{X}_{m,n} = \begin{bmatrix} \widehat{x}_1 & \widehat{x}_2 & \dots & \widehat{x}_n \\ \widehat{x}_2 & \widehat{x}_3 & \dots & \widehat{x}_{n+1} \\ \vdots & \vdots & \ddots & \vdots \\ \widehat{x}_m & \widehat{x}_{m+1} & \dots & \widehat{x}_{N-1} \end{bmatrix} \tag{21}$$

$$\overline{x}_1 = \frac{1}{k-l+1} \sum_{j=l}^{k} \mathbf{X}_{i-j+1,j}$$

$$l = \max(1, i-m+1)$$

$$k = \min(n, i)$$

For the two calibration parameters, it was considered m= 300 and l= 5 % of the first singular value for optimal performance, according to [48].

4.3. Investigation of the optimal performance

To establish AFDD's optimal performance, an effective MAC's threshold (α) should be defined to distinguish different mode shapes. In addition, several factors could significantly impact the accuracy and reliability of the modal identification. This research considered the acceleration record length, noise level, sensor's spatial resolution, the number of required modes within the predefined frequency range, and evaluated their impact on the modal identification through sensitivity analyses. These factors are commonly present in any SHM data acquisition campaign done with accelerometers and were chosen because operators can control them. Several other factors could have an impact on modal identification such as temperature, humidity, wind, heavy traffic, creep, shrinkage, material degradation, etc. To properly consider these factors, periodic or continuous monitoring data is needed. The use of existing benchmark datasets imposes certain limitations on the number and types of factors that can be included in the sensitivity analysis. In this research, the effect of using different MAC thresholds

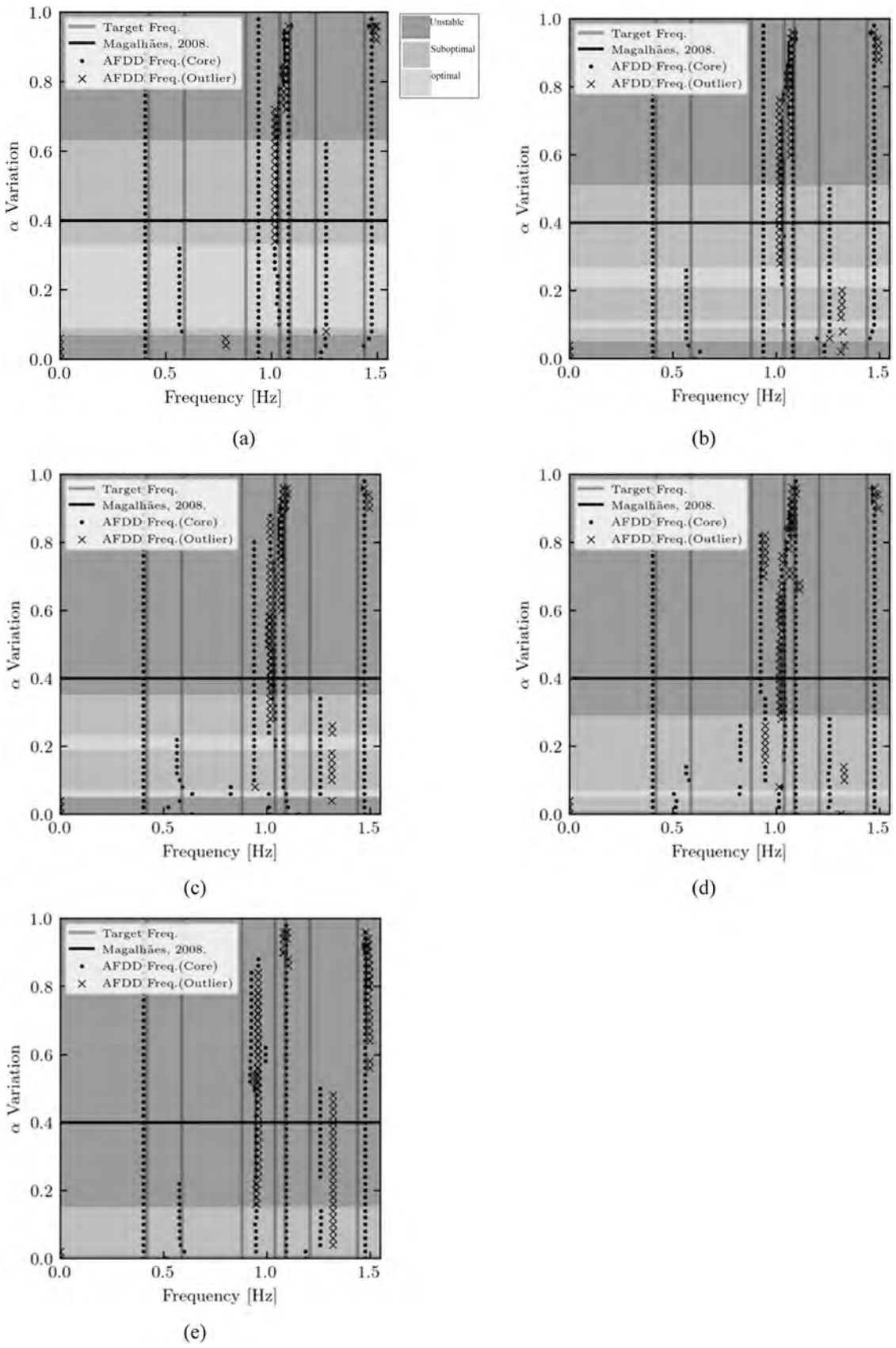

Fig. 6. The effect of α variation vs. the noise level: SVD denoising parameter (a) l= 0.05, (b) l= 0.20, (c) l= 0.35, (d) l= 0.50, (e) l= 0.75.

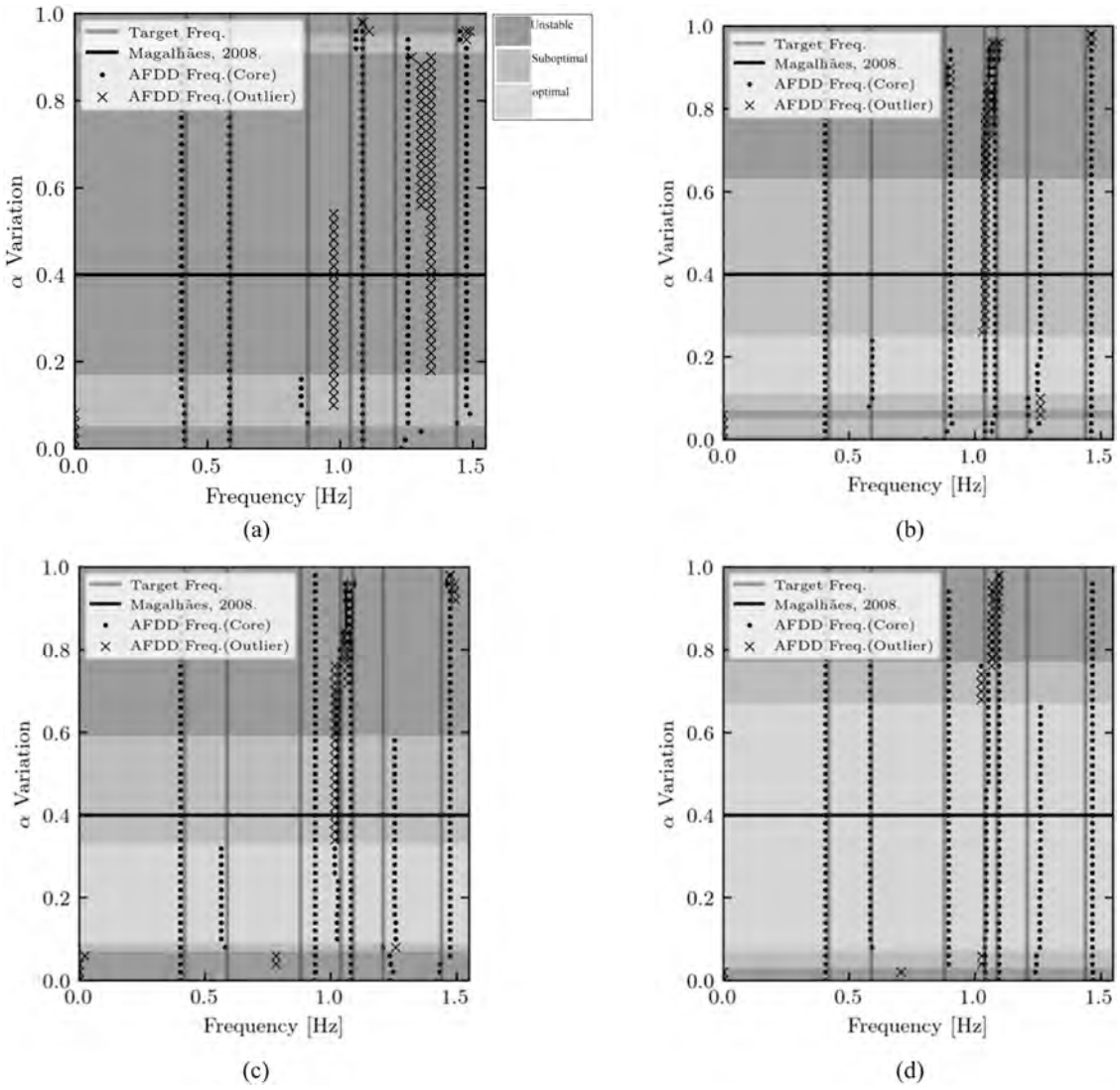

Fig. 7. The effect of α variation and signal length: Input duration of (a) 5 min, (b) 1 h, (c) 4 h, and (d) 12 h.

was investigated through several sensitivity analyses on the Yonghe cable-stayed bridge benchmark. The available data was related to a relatively short time window, which does not allow for considering the abovementioned additional factors. The acceptable ranges of MAC's threshold that result in optimal performance are obtained through stabilization diagrams comparing the AFDD's outputs to the FE model reference values of frequencies and modal shapes. First, the frequency range of interest and number of modes are defined. According to the outputs of the FE model, 7 frequencies and mode shapes should be identified in the 0–1.5 Hz frequency range. In each diagram, based on the number of misidentified modes, three different regions are identified, namely unstable, sub-optimal, and optimal. This was done utilizing a GMM algorithm to define a core and an outlier cluster in each stabilization diagram, as described in sections 2.1 and 2.3.

In the first sensitivity analysis, the MAC threshold α varies from 0 to 1, with a 0.02 increment. The frequencies identified by the AFDD algorithm are compared to the FE results in the stabilization diagram of Fig. 5. In the graph, AFDD estimates are reported on the horizontal axis, while the vertical axis represents the selected MAC's thresholds. Target frequencies obtained from the FE model are 0.42 Hz, 0.6 Hz, 0.88 Hz, 1.04 Hz, 1.09 Hz, 1.21 Hz, 1.44 Hz and they are indicated by vertical solid lines. The AFDD estimates that are included into the core cluster are scattered by solid circles. As it can be seen, the 0.42 Hz, 0.88 Hz, and 1.44 Hz target frequencies could be identified for almost any value of α. On the other hand, 1.04 Hz and 1.09 Hz frequencies were affected by the MAC threshold variation as other frequencies were picked by the algorithm, especially for α larger than 0.6. In this sensitivity analysis, the optimal area, where almost all frequencies are accurately estimated, falls within the range of α from 0.10 to 0.34. Notably, the value of $\alpha = 0.4$, suggested by [34], highlighted in the graph with a horizontal dashed line, falls within the suboptimal region and would have led to neglecting the 0.6 Hz frequency. It is also worth noting that the algorithm is able to clearly distinguish frequencies that are closely spaced as long as the selected α value falls within the optimal area.

In the second sensitivity analysis, the effect of different noise levels was investigated. Increasing the l parameter leads to higher noise levels in the output. Five cases were considered, setting the l parameter to 0.05, 0.20, 0.35, 0.50, and 0.75. Fig. 6 reveals that the regions of optimal and sub-optimal shrink as the noise level increases. In fact, when $l = 0.50$ and $l = 0.75$, it is no longer possible to define an optimal region. Modes with target frequencies of 0.88 Hz and 1.04 Hz were the most affected by noise and α variation. When $l = 0.05$, optimal noise reduction is achieved, and the optimal region is delimited by a MAC threshold ranging from 0.10 to 0.34 with the most accurate results within 0.18 to 0.22 Hz.

The third sensitivity analysis investigates the effect of the acceleration record length. In the literature different recommendations can be found. Cantieni (2005) recommended to consider a signal length

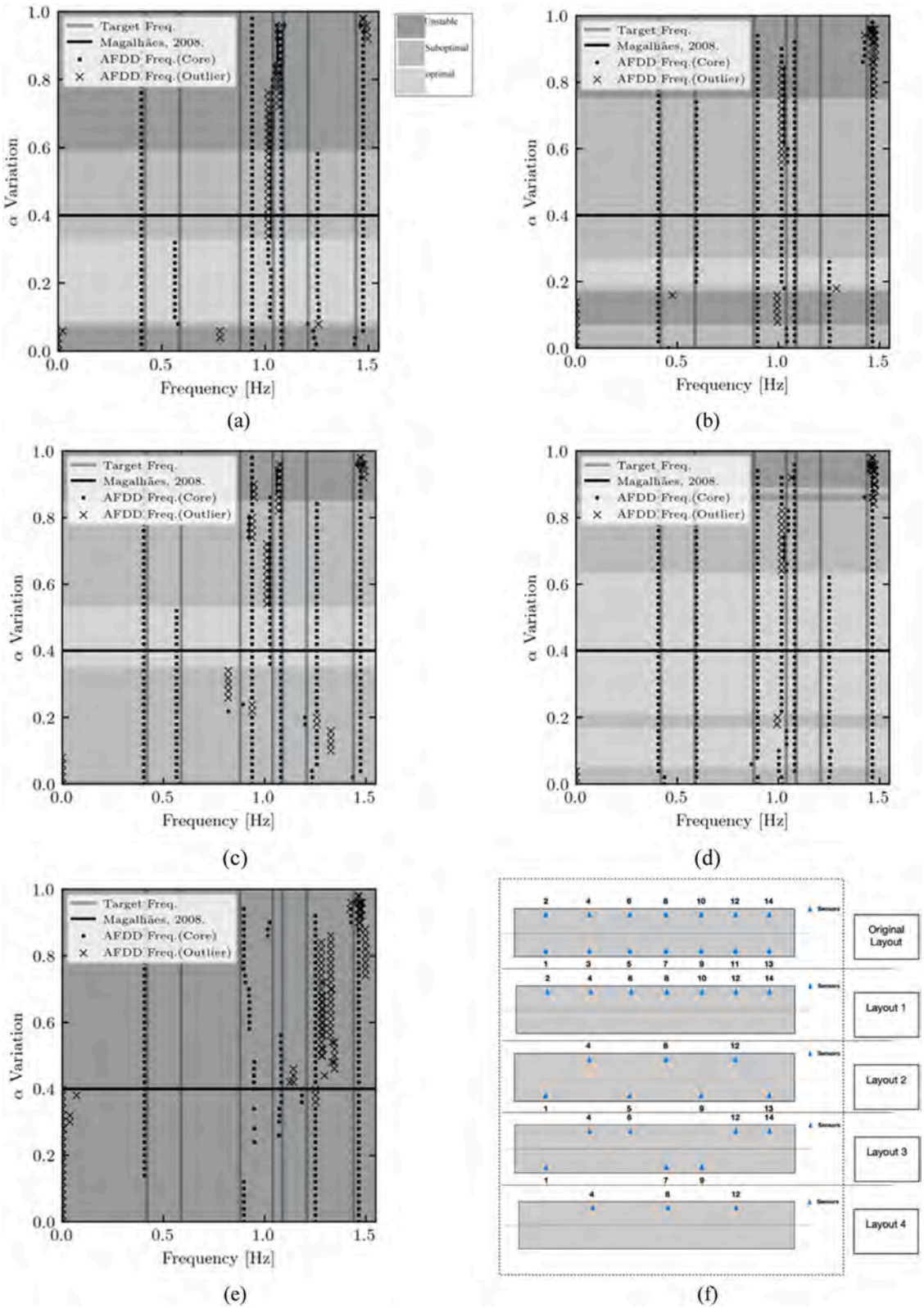

Fig. 8. The effect of α variation with the number of sensors and their layout: (a) original layout, (b) layout 1, (c) layout 2, (d) layout 3, (e) layout 4, (f) sensors layout.

exceeding 1000–2000 times the first natural period of the system [49]. For the Yonghe cable-stayed bridge, the natural period is approximately 2.40 s. This implies a record length between 40 and 80 min. Other studies argue that 15 to 60 min signals generally lead to accurate results [50]. In the seminal book by Brincker and Ventura [51] it is suggested to use signal durations greater than the ratio $10/(\xi f_{\min})$, where ξ is the damping ratio and f_{min} the lowest natural frequency of the system. In our case the lowest natural frequency is 0.42 Hz, and the corresponding damping ratio is 6.84 % as reported in [43]. Thus, the signal length should be greater than 3480 s or 58 min.

Based on these recommendations, the effect of α variation is analyzed for signals with length of 5 min, 1, 4, and 12 h (Fig. 7).

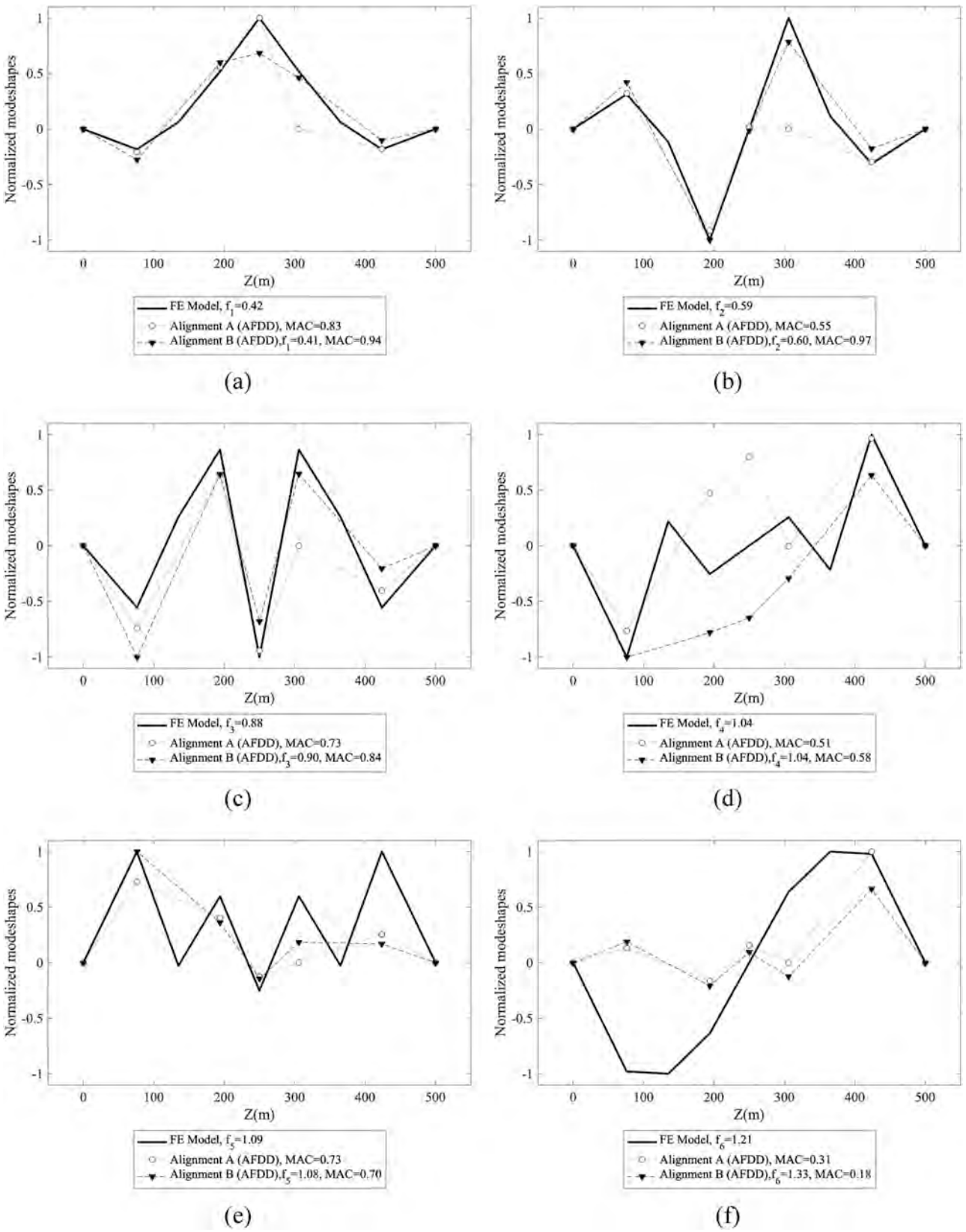

Fig. 9. Mode shapes obtained from layout L3 with $\alpha = 0.24$.

Commonly, longer signal durations offer a finer resolution to capture the dynamic characteristics of a structure, leading to more reliable frequency estimations. Indeed, the optimal region widens as the signal length increases and the most inaccurate results correspond to a duration of 5 min. However, anomalies might still occur. For instance, as seen in Fig. 7b and Fig. 7c, although the optimal region widens, the precision of estimating the target frequency of 0.59 Hz decreases. This could be attributed to peculiar characteristics of the ambient vibrations

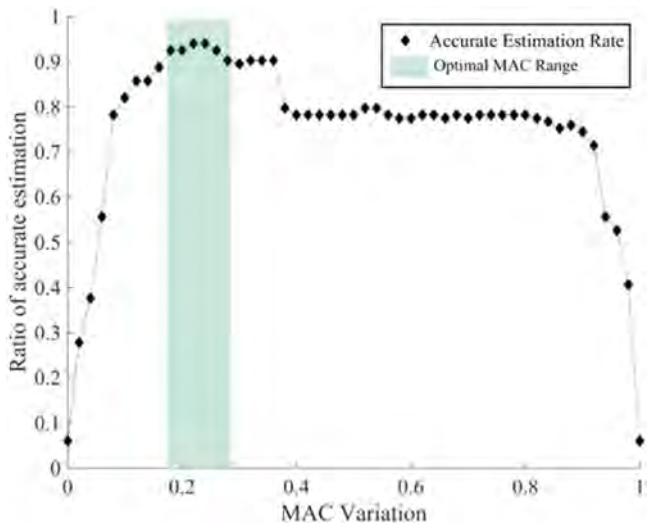

Fig. 10. Ratio of correct estimation for each α value.

and their intensity at the moment of recording. Nonetheless, the analysis shows that selecting an appropriate α value, it is possible to obtain accurate results with 1-hour records. This approach could be helpful to designing monitoring campaigns, potentially reducing their cost by determining a proper duration. It is worth mentioning that record length is here intended as a parameter that allows to carry out a single analysis, showing the modal properties related to a specific time and date. To fully assess the long-term stability of the bridge, this assessment should be repeated over a long time through periodic or continuous monitoring. Any significant deviations of the modal parameters from the baseline values could indicate changes in the global dynamic behavior.

In the fourth sensitivity analysis, the effect of reducing the number of sensors and changing their location was evaluated. Sensor location is extremely important to be able to identify correct mode shapes. The number of sensors and their layout are usually well studied before starting a monitoring campaign. If sensors are not well positioned, the results that can be obtained from OMA are inevitably going to be incomplete. To investigate this aspect, five different sensor layouts were considered as shown in Fig. 8f. In the original layout, used during the monitoring campaign, 7 sensors were placed on each side of the bridge deck. Layouts 1 to 4 consider different combinations with a lower number of sensors. Fig. 8 shows that the optimal region varies greatly depending on the sensor placement and when only three sensors were considered (layout 4) an optimal region could not be identified. Nonetheless, it is worth noting that across all layouts, the modes with target frequencies 0.42 Hz and 1.44 Hz are less affected by the sensor spatial resolution and could always be detected given that these modes have higher mass participation factors.

Changing the number of sensors and their layout has an effect not only on the ability of detecting frequencies, but also on the quality of the mode shapes. To further discuss this point, an additional series of analyses were carried out. Based on the general rule that sensors placed nearby the maximums and minimums of the mode shapes have more chance of capturing the structural dynamics, three layouts where sensors are located close to the maximums and minimums of the first three modes were investigated. It was chosen to keep the layouts symmetric with respect to the middle axis to account for possible differences in the excitation levels at the two sides of the bridge deck. The top alignment is referred to as alignment A and the bottom one as alignment B. The location of maximums and minimums was extracted from the reference FE model. The first layout included sensors no. 1, 2, 7, 8, 13, 14. The stabilization diagram obtained iterating the AFDD analysis varying the α threshold showed that all α values were unstable except for a suboptimal scenario for $\alpha = 0.34$. The seventh frequency equal to 1.44 Hz could not be identified. Except for the first mode, the obtained deformed shapes were far from the actual ones. Even when the modal coordinates are comparable to those coming from the FE model, the lack of sensors leads to neglecting peaks of deformation in between the sensors. In this case, a high MAC value alone is not indicative of a good matching with the actual mode shape. Similar results were achieved when considering the second mode shapes, which shows four peaks. In this case, sensors no. 1, 2, 5, 6, 9, 10, 13, 14 were part of the second layout. The AFDD was now able to detect the 7 frequencies for α ranging from 0.21 to 0.24. However, several issues appeared by looking at the mode shapes. Given the malfunctioning of sensor no. 10 in alignment A, the only mode shape that was well captured by alignment B was the one of the second mode.

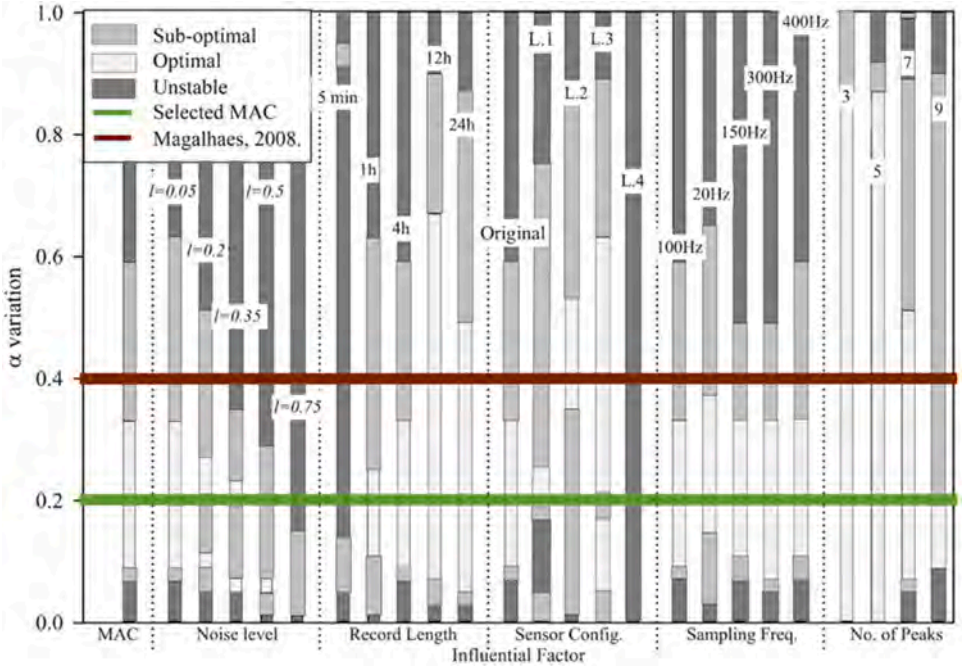

Fig. 11. The sub-optimal/optimal ranges derived from sensitivity analysis for each case.

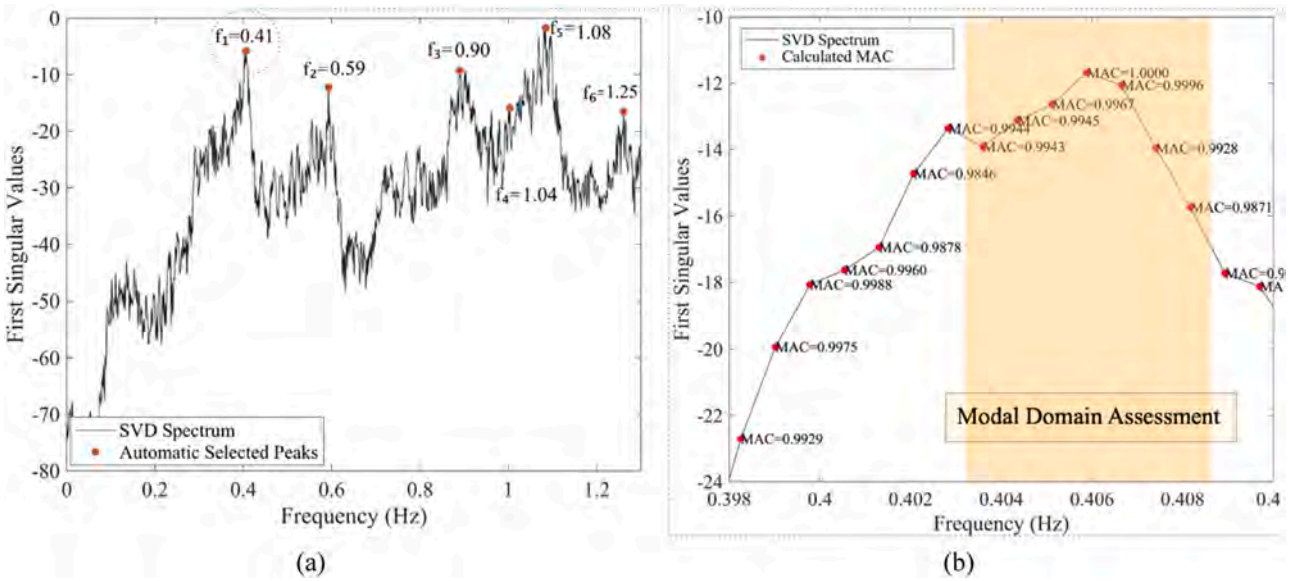

Fig. 12. AFDD analysis of the cable-stayed bridge for 1-hour signal: (a) selected peaks in the SV spectrum, and (b) MAC evaluation for the first selected peak and modal domain assessment.

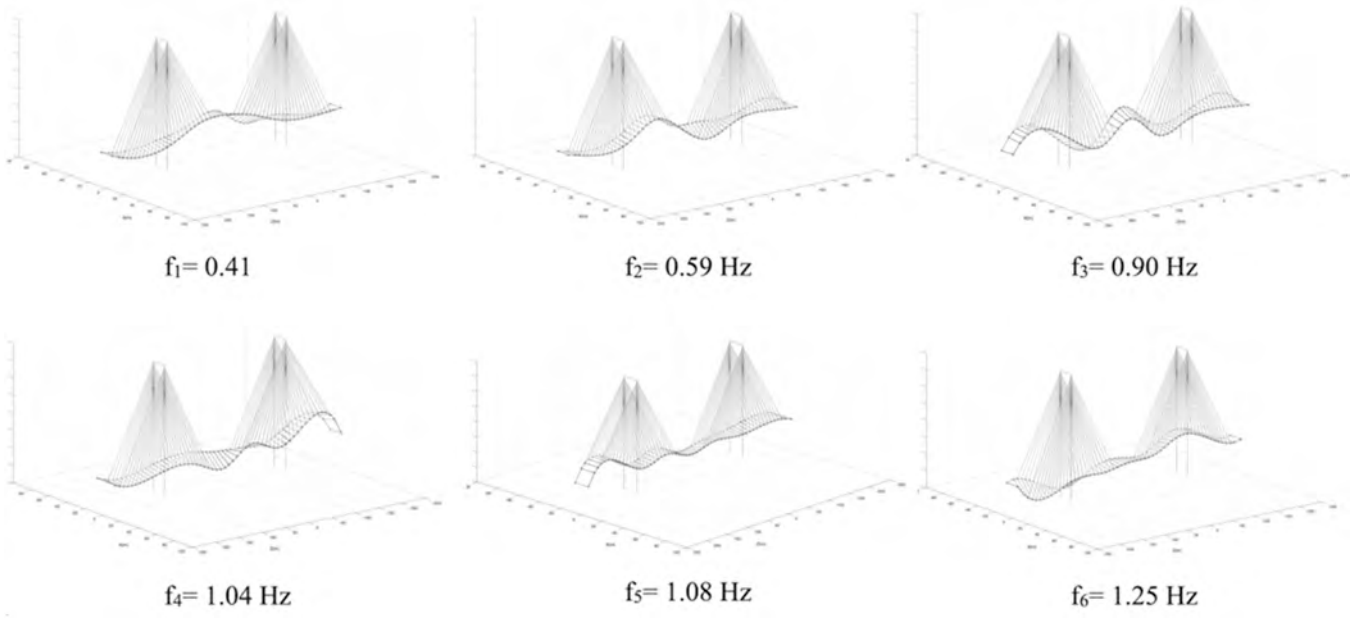

Fig. 13. 3D deformed configuration of the Yonghe cable-stayed bridge.

The third mode is characterized by 5 peaks, thus two alignments with 5 sensors each were considered (no. 1, 2, 5, 6, 7, 8, 9, 10, 13, 14). Effectively, the third layout (L3) is a superimposition of the first two. However, the sixth and seventh modes could not be identified at the same time, meaning that only sub-optimal regions were found. The mode shapes corresponding to a suboptimal $\alpha = 0.20$ are plotted in Fig. 9. The improvement that is seen with this sensor layout is that the first three modes shapes are captured quite reasonably.

These results suggest that a sparse sensor grid with a limited number of sensors might be enough to get most of the predominant frequencies of the structure. Nonetheless, the mode shapes related to those frequencies contain only partial information and by assuming them as correct the understanding of the structural dynamics would be considerably compromised. Strategic sensor placement is essential and a preliminary analysis to determine where the maximums and minimums deformation points could be located is always desirable.

The sampling frequency of the sensors and the number of output frequencies are additional factors that were considered in the sensitivity analyses. The sampling frequency should be chosen based on an adequate number of cycles of the fundamental or target modes to ensure that the dynamic response of the structure is accurately represented. According to Brincker and Ventura [51], it is advisable to select a sampling frequency at least 2.4 times greater than the maximum frequency of interest. For the Yonghe cable-stayed bridge, the frequency range 0–1.5 Hz is enough to cover the main structural dynamics, including the fundamental and higher modes. Therefore, the sampling frequency should be greater than 3.6 Hz. However, it is common practice to use commercial sensors with much higher sampling frequencies. In this application, the original records were sampled at 100 Hz. To simulate the use of different sensors, these were downsampled at 20 Hz

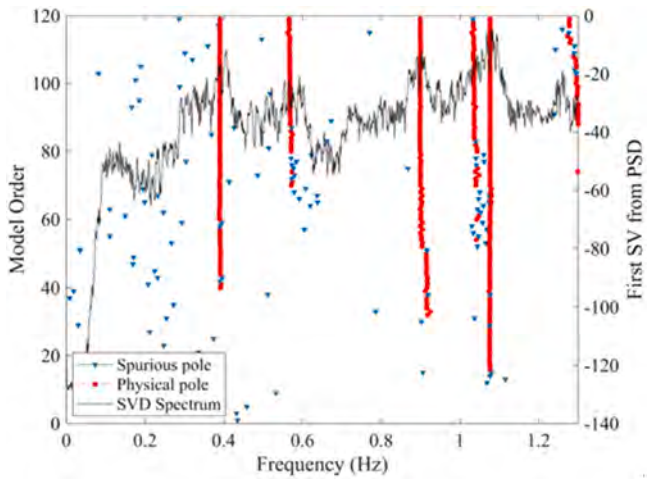

Fig. 14. Stabilization diagram of the cov-SSI analysis of the Yonghe cable-stayed bridge for 1-hour record.

and upsampled at 150 Hz, 200 Hz, 300 Hz, and 400 Hz. Predictably, it was found that the optimal region is barely affected by the sampling frequency change. Therefore, even a 20 Hz sampling sensor would be enough to obtain comparable results, without the need for more expensive sensors sampling at higher frequencies.

As far as the number of output frequencies is concerned, the sensitivity analysis considered 3, 5, 7, and 9 output values. Results showed that when the number of outputs is set to a value lower than the actual number of frequencies, the optimal region expands, and the algorithm identifies modes with higher mass participation factors. However, when 9 outputs are selected, modes with zero-valued natural frequency are observed for an α value lower than 0.2.

A plot illustrating the accuracy of AFDD estimates across all analyses is presented in Fig. 10. For each value of α in the horizontal axis, AFDD outcomes are compared to the target frequencies and deemed correct if the difference is less than 0.1 Hz. Then, the number of correct estimations is divided by the total AFDD analyses performed to get the ratio of correct estimations for each α value. It can be observed that the optimal performance could be achieved with a MAC in the range of 0.18 - 0.24.

In addition, Fig. 11 summarizes the optimal, suboptimal, and unstable regions for all the performed sensitivity analyses. It is seen that the horizontal line with the MAC= 0.2 cross high number of optimal regions. Therefore, in the following sections, the proposed AFDD methodology is applied to three case studies considering a MAC threshold $\alpha = 0.2$. This value differs from the previous findings of Magalhães et al. [34], where the suggested MAC threshold was 0.4. Furthermore, in the rest of this study, a modal domain assessment is conducted to verify that the selected peak in the SV spectrum is associated with a physical mode. The verification is done by considering 7 points in the spectrum and checking that the mean MAC is 0.6 or higher.

5. Validation of the AFDD procedure

In this section, the optimized AFDD procedure is tested on three inherently different case studies. To validate the methodology, cov-SSI, and traditional FDD are applied to each case study, and the results are compared in terms of modal properties.

5.1. Case Study 1: Yonghe cable-stayed bridge

The first case study is the previously described Yonghe cable-stayed bridge. The vertical acceleration records, plotted in Fig. 3b, collected from 03:00 a.m. to 04:00 a.m. on January 17, 2008, were used to test and validate the AFDD procedure. Considering the 0–1.3 Hz frequency range, the number of desired outputs was set to 6, as the number of frequencies resulting from the FE model. Fig. 12a. shows the peaks automatically selected in the SV spectrum and the corresponding identified modal frequencies after performing the AFDD analysis. The MAC variation is illustrated for the first identified peak in Fig. 12b.

The modal domain assessment considers six SV points in the selected domain around the identified peak. Modes are considered physical if the

Table 2
Comparison of the Yonghe cable-stayed bridge frequencies obtained through different methods.

FE model [Hz]	FDD, Li et al. [43] [Hz]	Cov-SSI (1 h) [Hz]	AFDD (1 h) [Hz]	Cov-SSI (12 h) [Hz]	AFDD (12 h) [Hz]
0.42	0.42	0.39	0.41	0.39	0.41
0.59	0.59	0.56	0.59	0.58	0.59
0.88	0.89	0.90	0.90	0.90	0.89
1.04	1.04	1.03	1.04	1.02	1.05
1.09	1.10	1.08	1.08	1.08	1.09
1.21	1.27	1.28	1.25	1.26	1.26

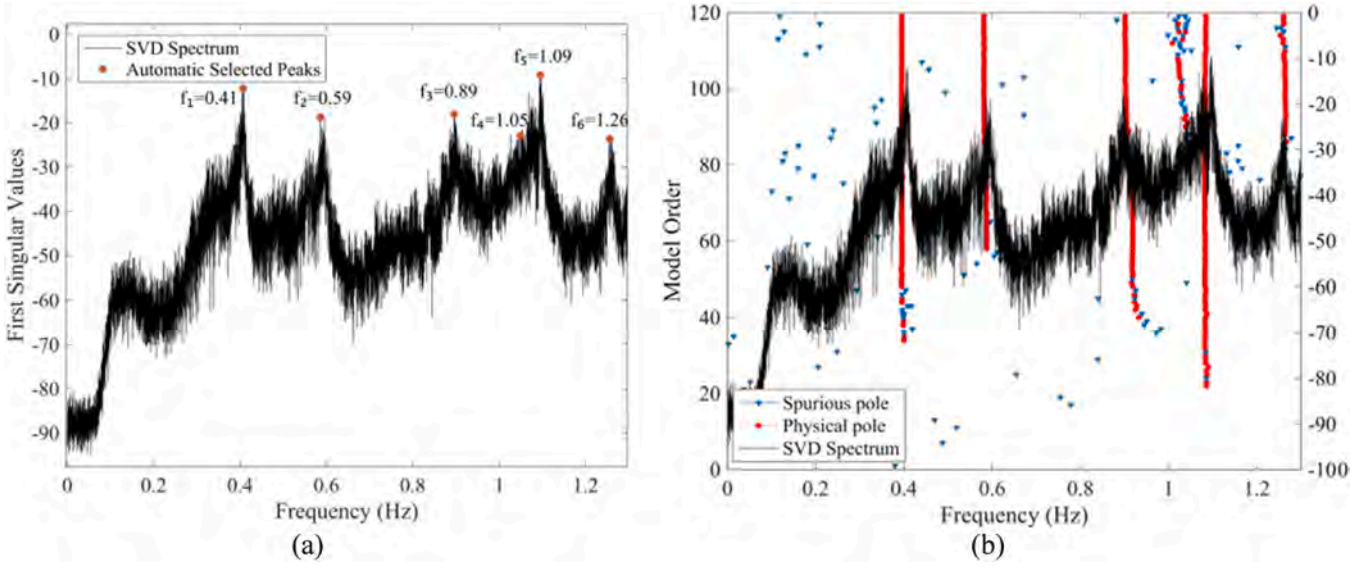

Fig. 15. (a) AFDD analysis of the cable-stayed bridge (12 h), (b) Stabilization diagram of the Yonghe cable-stayed bridge (12 h).

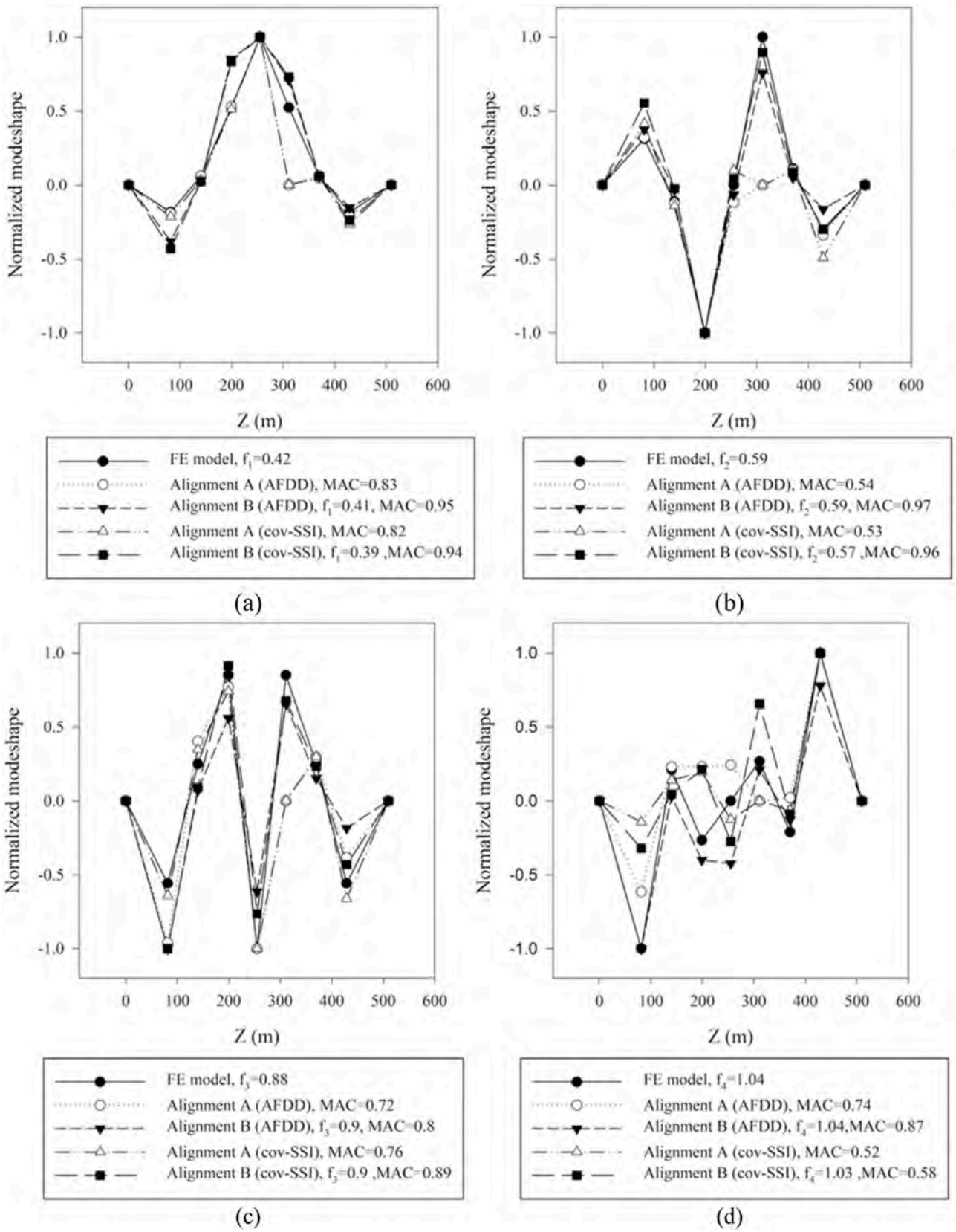

Fig. 16. Comparison of derived mode shapes for Yonghe cable-stayed bridges (1-h duration), (a) 1st mode, (b) 2nd mode, (c) 3rd mode, (d) 4th mode, (e) 5th mode, (f) 6th mode.,.

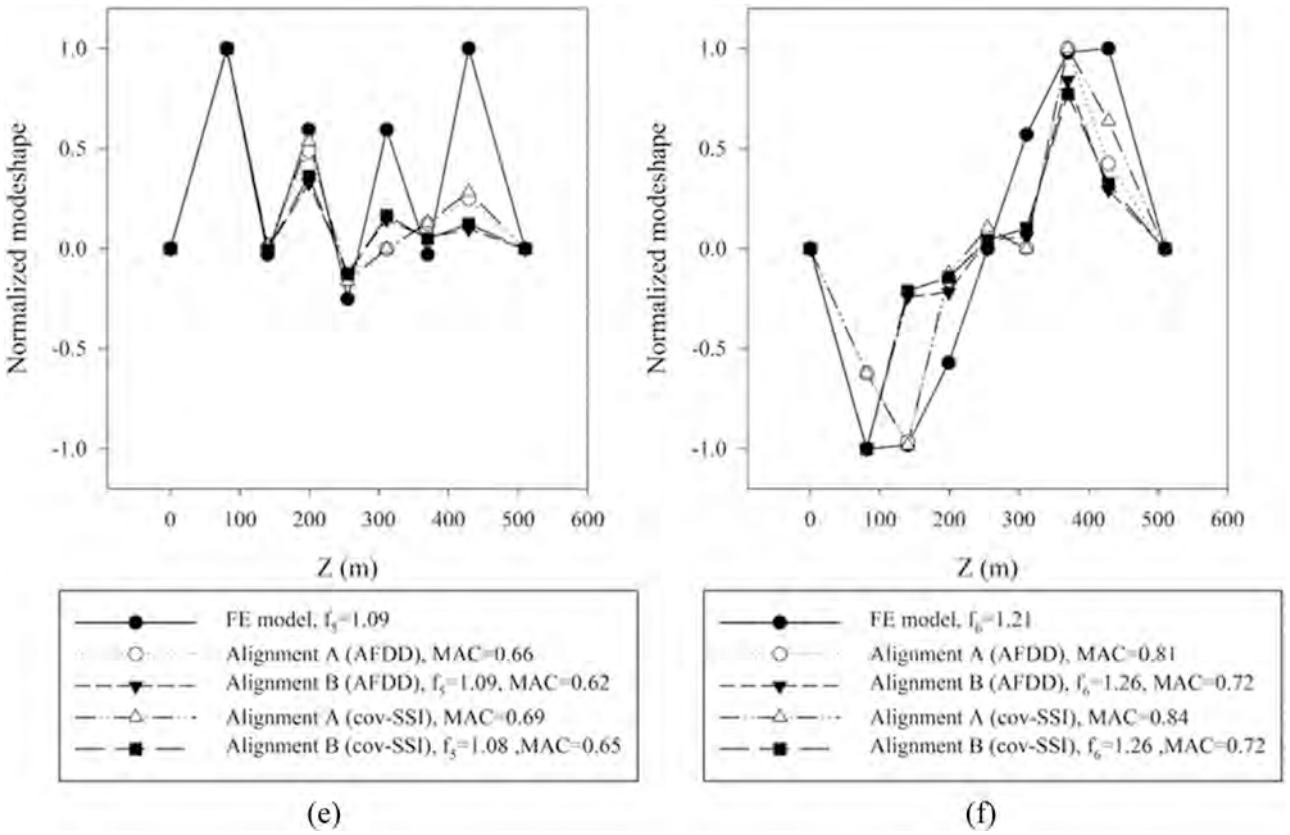

Fig. 16. (*continued*).

mean MAC computed from the SV points exceeds the predefined threshold of 0.6. In this case study, the mean MAC is significantly larger than the applied threshold. Since in the proposed AFDD method the identification of dynamic modes is not only based on amplitude in the SV spectrum but also on the geometry of the mode shape, it is possible to identify even low-amplitude frequencies that are relevant to the dynamics of the structure. The 3D vertical mode shapes obtained from the AFDD are illustrated in Fig. 13. The mode shapes were drawn through a spline interpolation between the sensor locations.

Subsequently, the cov-SSI analysis was performed. The time lag was set to 366, and the model order to 120 following the recommendations by Zhou et al. [39]. Fig. 14 shows the stabilization diagram, which features six clear alignments of poles. These poles are referred to as stable and highlighted in red. The corresponding frequencies are $f_1 = 0.39$ Hz, $f_2 = 0.56$ Hz, $f_3 = 0.90$ Hz, $f_4 = 1.03$ Hz, $f_5 = 1.08$ Hz, $f_6 = 1.28$ Hz.

The analysis was repeated for an additional signal recorded from 01:00 a.m. to 12:00 p.m. on January 17, 2008, using the same parameters described for the 1-hour record. The automatically selected peaks and identified frequencies are presented in Fig. 15a. Here, since the record length increases, the windows segmentation and the number of points used for the Fast Fourier Transform of the input signal to derive the PSD increase, leading to a denser SV spectrum with more chances of selecting non-physical modes. Nonetheless, the AFDD performed accurately. On the other hand, from the cov-SSI analysis it was possible to clearly identify 5 stable modes with frequencies $f_1 = 0.39$ Hz, $f_2 = 0.58$ Hz, $f_3 = 0.90$ Hz, $f_5 = 1.08$ Hz, $f_6 = 1.26$ Hz, and one semi-stable mode with frequency $f_4 = 1.02$ Hz (Fig. 15b).

The comparison among previous research, OMA methodologies, and FE modal analysis is presented in Table 2. Within the frequency range of 0–1.3 Hz, all methodologies were able to identify six frequencies with similar values. Regarding the 1-hour record, the AFDD results were closer to the FE model frequencies compared to those obtained from the cov-SSI approach. In the case of the 12-hour signal, the AFDD also performed slightly better.

To evaluate the consistency of the mode shapes extracted by the different methods, they were plotted in Fig. 16, separating the results corresponding to sensor alignments A and B. In each plot, the modal coordinates are normalized by the maximum magnitude and the horizontal axis specifies the sensor location. The MAC values were calculated between the obtained modes and the FE counterparts for each sensor alignment and OMA methodology. Notably, larger MAC values characterize the mode shapes resulting from the AFDD analysis compared to cov-SSI estimates. This is particularly pronounced for the fourth mode Fig. 16d. While the obtained mode shapes exhibit reasonable coherence, some unusual deviations can be observed. On one hand, the distortions seen around sensor No.10, located at 350 m, are clearly due to a malfunction, visible from the raw data both in the time and frequency domains. Moreover, differences could be due to the fact that the FE model considers the longitudinal middle axis of the bridge, whereas the sensors are placed on the sides of the deck.

This application showed that the optimized AFDD produced accurate results, and the risk of selecting spurious peaks in identifying vertical modes of vibration decreased compared to the cov-SSI method.

5.2. *Case Study 2: PolyU Footbridge*

The PolyU footbridge is an irregular structure with butterfly-shaped steel tube arches located at Hong Kong Polytechnic University. It consists of a primary and two side spans with a length of 84.24 m and 64.26 m, respectively, supported by hangers connected to two inclined arches. An SHM system was installed on the footbridge during the construction phase and started acquiring data on September 28, 2019. The system includes three-axial and uniaxial accelerometers, spatially distributed optic sensors, FBG sensors, and a global navigation system. The accelerometers, with a sampling frequency of 50 Hz, are mounted

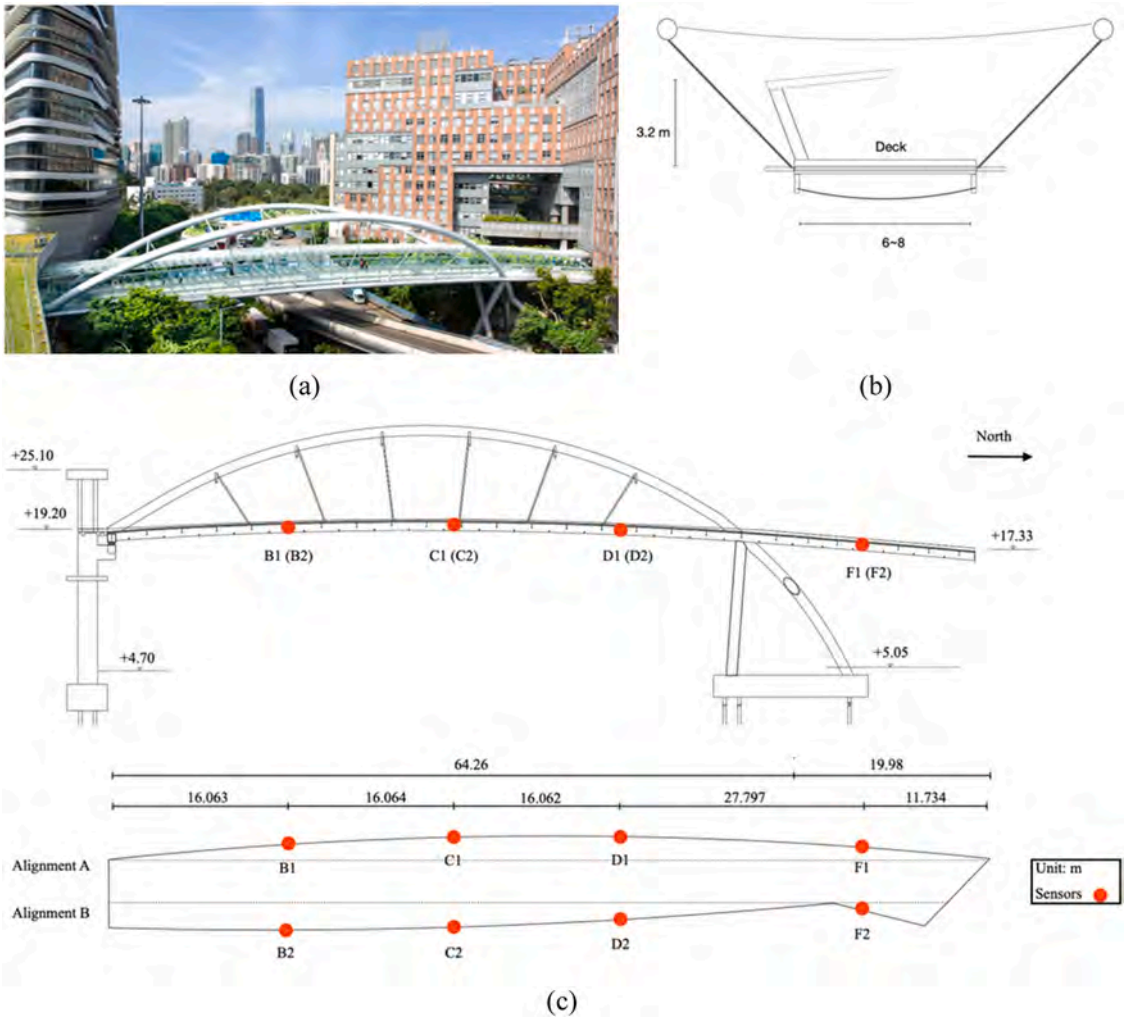

Fig. 17. (a) PolyU footbridge, (b) cross-section, (c) side view and sensor layout.

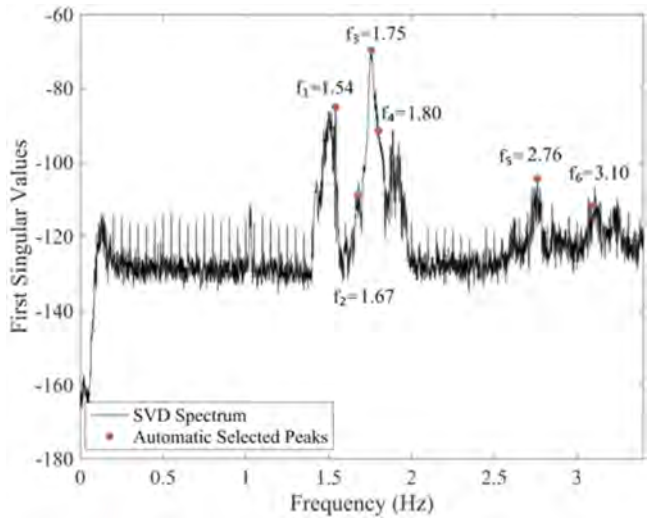

Fig. 18. The automatically selected peaks in the SV spectrum by the AFDD algorithm.

on the sides of the deck along two alignments, as illustrated in Fig. 17. The sensors placed along alignment B are three-axial, whereas those along alignment A can record only vertical accelerations.

A 3D FE model of 8785 elements was developed to simulate the dynamics of the bridge and calibrated according to the modal properties acquired from the SSI method. The FE analysis revealed the presence of combined vertical and torsional mode shapes [19]. The modal properties obtained through the FE modal analysis and SSI were compared to the results obtained with the proposed AFDD methodology. The ambient vibrations recorded from 00:00 a.m. to 01:00 a.m., November 1, 2019, were used. For the AFDD analysis, the frequency range of interest was fixed to 0–3.2 Hz and the number of desired outputs to 6. Fig. 18 highlights the six frequencies automatically detected by the AFDD procedure. It is worth noting that thanks to the implemented features of the algorithm, it is possible to select relevant frequencies even when there are not obvious peaks, like in the case of $f_2 = 1.67$ Hz and $f_4 = 1.80$ Hz. This would not be possible with the traditional FDD technique.

Fig. 19 presents the 3D mode shapes identified using AFDD. The modes at 1.54 Hz, 1.75 Hz, and 1.80 Hz result from combinations of lateral and vertical dynamic modes. The mode at 1.67 Hz is a torsional mode, and the one at 2.76 Hz combines transversal and torsional deformations.

In the cov-SSI analysis, the system order was set to 100 following the work done by Xia et al. [19], while the time lag was set to 65 since the fundamental frequency is 1.16 Hz. The stabilization diagram is plotted in Fig. 20, which shows the presence of 5 stable modes, although not all of them formed clear vertical alignments, corresponding to the following natural frequencies: $f_1 = 1.5$ Hz, $f_2 = 1.75$ Hz, $f_3 = 1.78$ Hz, $f_4 = 1.91$ Hz, $f_5 = 2.75$ Hz. It is worth noting that many factors, such as

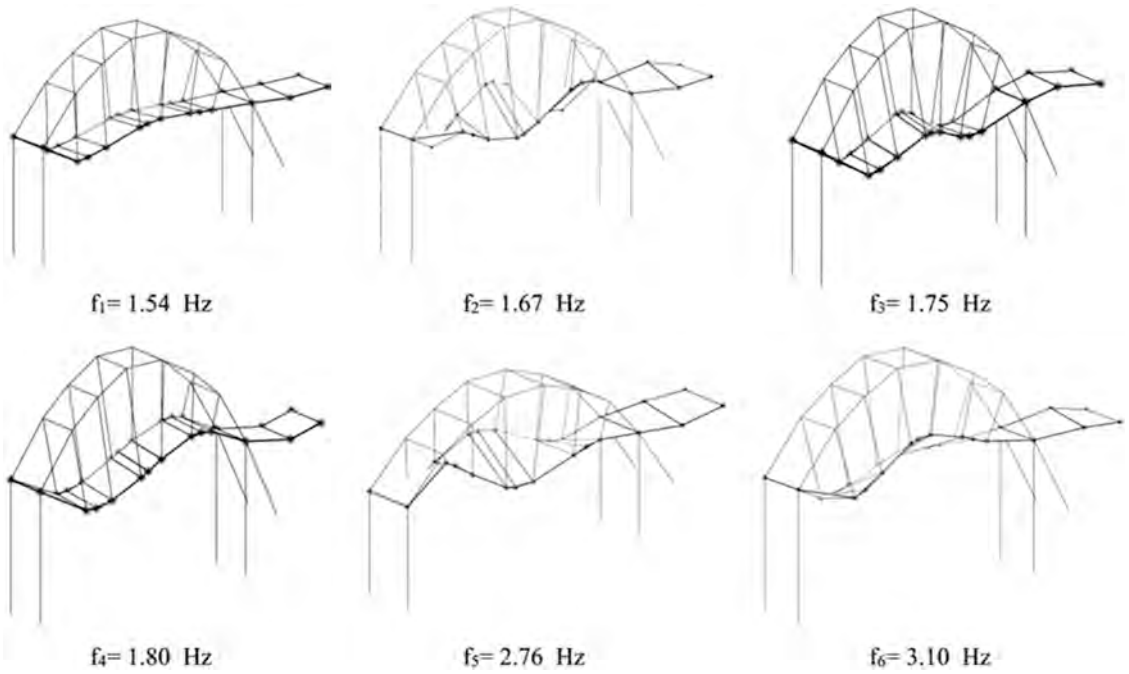

Fig. 19. 3D mode shapes of the PolyU footbridge identified through AFDD.

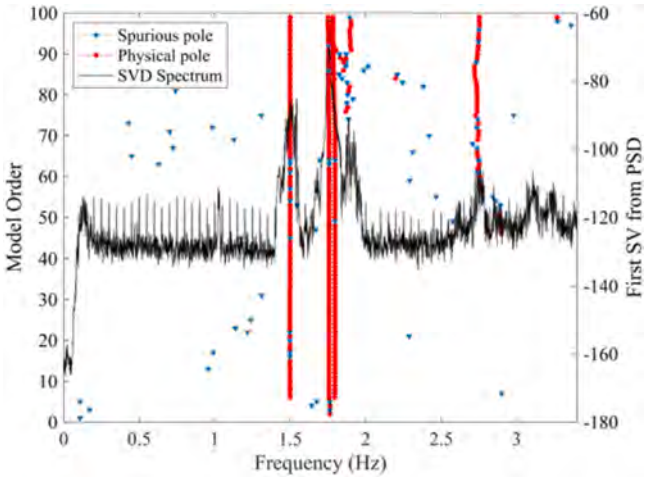

Fig. 20. Stabilization diagram for the PolyU footbridge.

noise, signal quality, and data preprocessing, can introduce small variations that prevent perfect vertical alignments from occurring. Moreover, as described in Section 3.2, the chosen stabilization criteria are quite stringent. While this approach helps in filtering out spurious modes, it also increases the likelihood of rejecting modes that may otherwise appear stable under less stringent conditions. In Fig. 20, it is possible to see a single pole appearing around 3.3 Hz. This is most likely a mode with a weak energy contribution to the overall system response. Hence, it was not considered in the analysis.

Table 3 reports the frequencies obtained from AFDD and cov-SSI and those from the 2019 study of Xia et al. [19]. The characteristics and direction of each mode shape are also clarified based on the 3D deformed geometry. In the 2019 study, four mode shapes were identified within the 1.8–3.10 Hz frequency range. The current study produced different results. The AFDD analysis identified 6 modes and the cov-SSI analysis identified 5 stable modes. The cov-SSI encountered limitations in capturing two modes: (i) the deck torsion with frequency of 3.10 Hz encountered both in the previous study and AFDD, (ii) the

Table 3
Comparison of the PolyU footbridge frequencies obtained through different methods.

FE [Hz]	SSI (2020) [Hz]	Description	AFDD [Hz]	Description	Cov-SSI [Hz]
1.80	1.88	Deck vertical	1.54	Combination of vertical and lateral on the half of the bridge	1.50
2.04	1.94	Deck torsional	1.67	Deck torsional, symmetrical is *x*-dir, skew sym. in *y*-dir	-
2.81	2.63	In-plane bending lateral	1.75	Combination of vertical and lateral and torsional	1.75
2.97	3.10	Deck torsion	1.80	Vertical, skew symmetrical	1.78
-			-	Deck torsional	1.91
			2.76	Transversal and torsional	2.75
			3.10	Torsional	-

torsional mode with frequency of 1.67 Hz, detected by the AFDD analysis. Conversely, the AFDD excluded the deck torsional mode with frequency of 1.94 Hz. It was found that the torsional mode is not identified since its shape is similar to the vertical mode with a frequency of 1.80 Hz. Indeed, the MAC calculated between them is 0.74. A viable solution to this issue would using more sensors and a better placement.

The AFDD and cov-SSI analyses revealed the presence of respectively 3 and 2 new modes below 1.80 Hz, which was the first frequency based on the FE model. Since the acceleration records are not the same used in the previous work, the newly identified modes might be associated with an additional vibration source. However, this would require further investigation, which is beyond the scope of the current study. The mode shapes obtained through the AFDD and cov-SSI methods for alignments A and B are plotted in Fig. 21 where the *x*-axis corresponds to sensor locations, and the *y*-axis to modal values normalized by the highest magnitude. In this case, it was not possible to compare the results to the FE model for confidentiality reasons. Therefore, the MAC was calculated only between the modal vectors obtained through AFDD and cov-SSI. The consistency observed for the modes with frequencies below

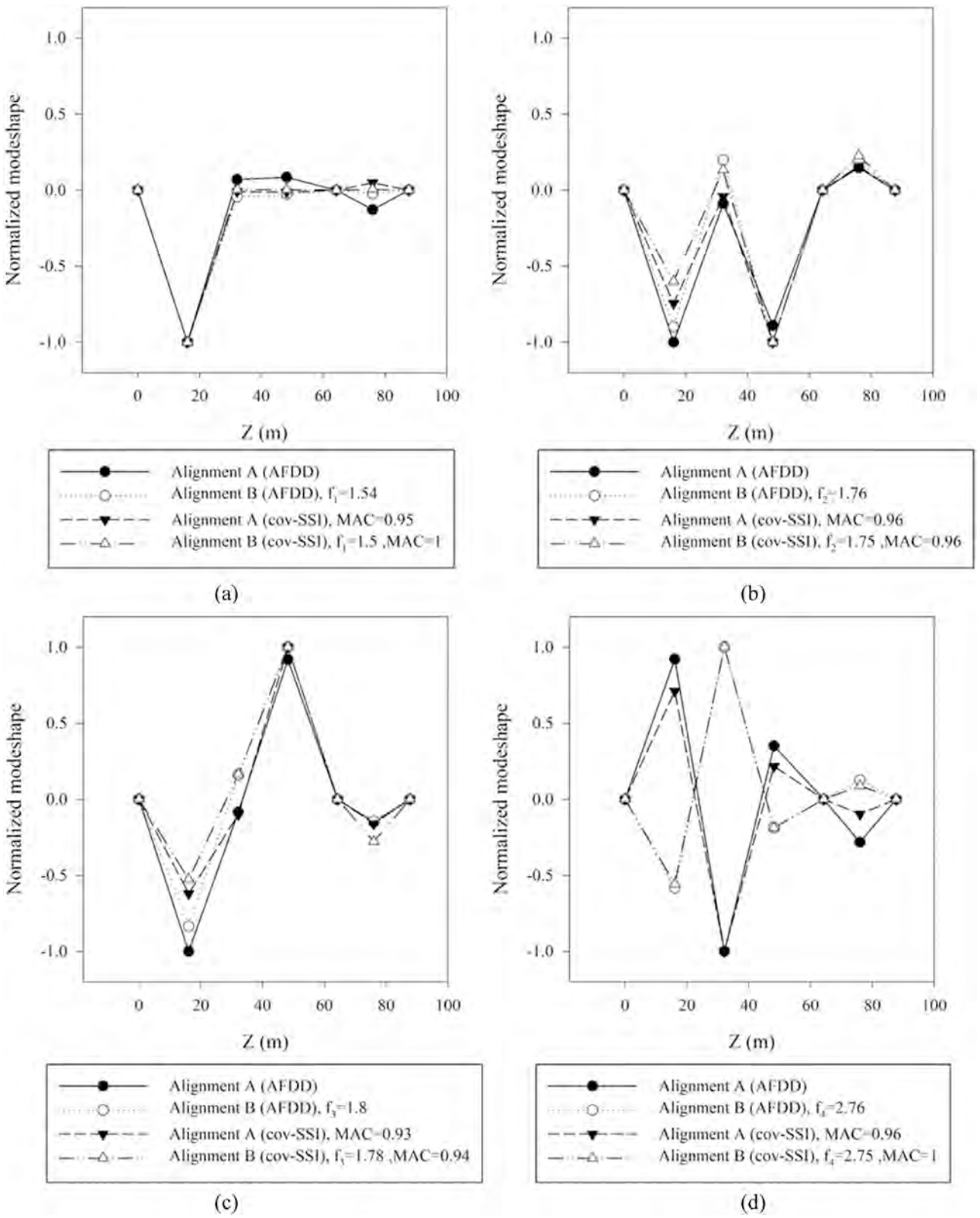

Fig. 21. Comparison of extracted mode shapes from PolyU footbridge, (a) first mode, (b) second mode, (c) third mode, (d) fourth mode.

1.8 Hz further indicates they are not attributable to a miscalculation or noise in the input signal. Overall, the highest consistency was observed for the 2.76 Hz mode.

In conclusion, when identifying torsional modes using the optimized AFDD, there are two main aspects to consider. First, the modal domain, where a gradual change of MAC occurs, is narrower for torsional modes. In other words, in the automated peak piking algorithm, there is a rapid transition in the MAC value that might go from 0.2 to 1 around a peak associated with a torsional mode. This means that the method demands flexibility in setting the threshold regarding the number of SV points and

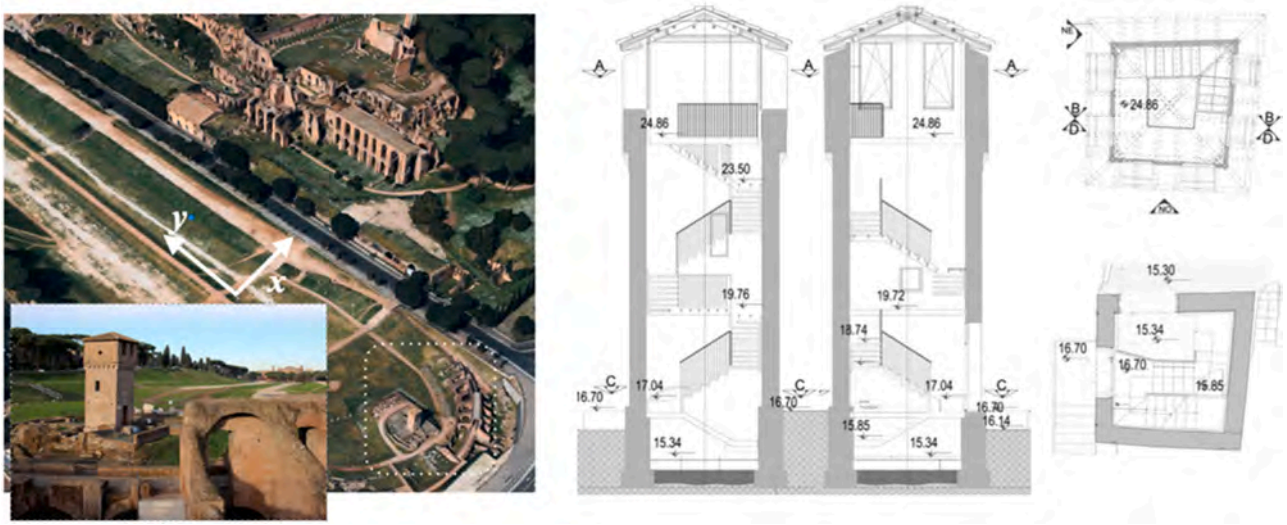

Fig. 22. Aerial view of the Circus Maximus and drawings of the Moletta tower.

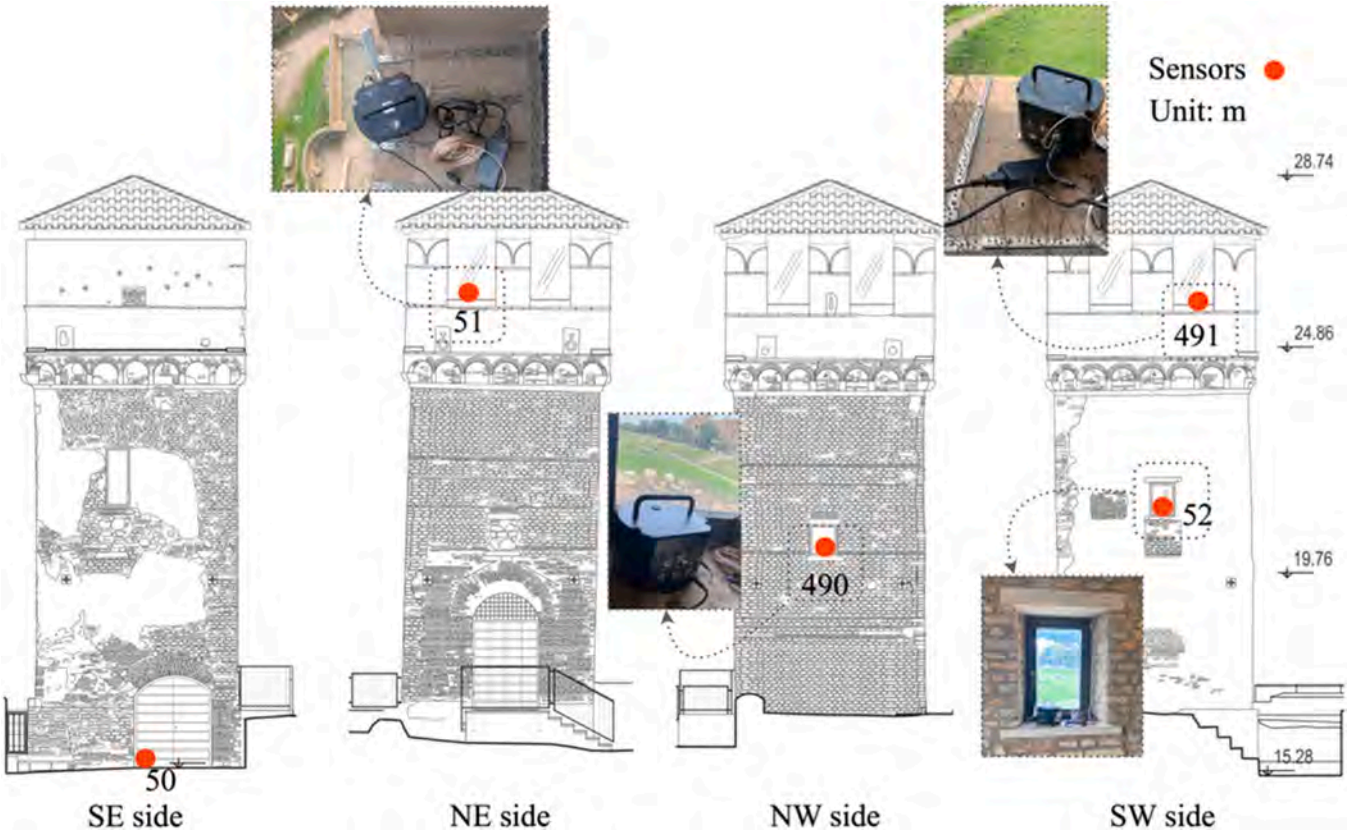

Fig. 23. Sensor placement on the Moletta tower.

MAC mean in the modal domain assessment. For this reason, a narrow modal domain with six SV points and a MAC mean value of 0.6 were predefined in the methodology to prevent errors in neglecting torsional modes. Secondly, the identification of modes that combine torsion and translation may be challenging because of the similarity of their geometries. Therefore, it requires optimal sensing strategies and sensor placement to be able to capture the proper dynamics of the structure.

5.3. *Case study 3: Moletta tower*

The third case study is the Moletta tower, a medieval tower part of the Circus Maximus archaeological site in Rome, Italy. The Circus Maximus was built in the first half of the sixth century BC and hosted ancient Roman chariot-racing tournaments. The original track level is buried under 9 m of soil, creating a complex soil-structure interaction. Nowadays, the venue hosts concerts and entertaining events, such as the Rolling Stones concert in 2014 and more recently the Bruce Springsteen concert in 2023 with an estimated attendance of over 70,000 people.

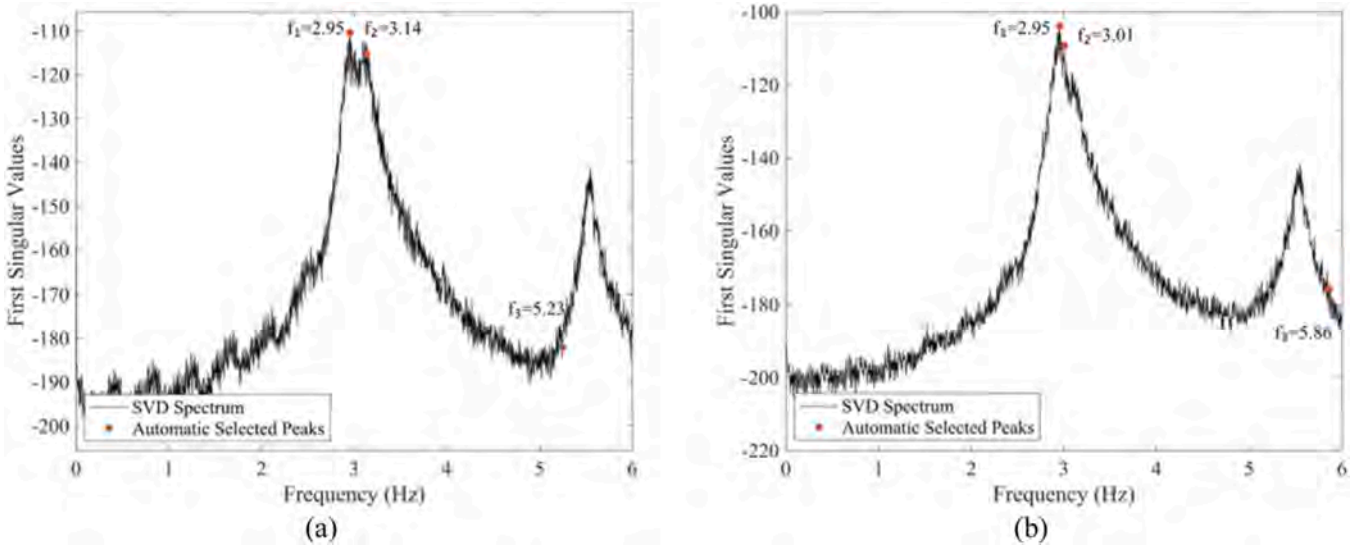

Fig. 24. SV spectra and automatically selected frequencies by the AFDD algorithm in (a) *x*-direction and (b) *y*-direction.

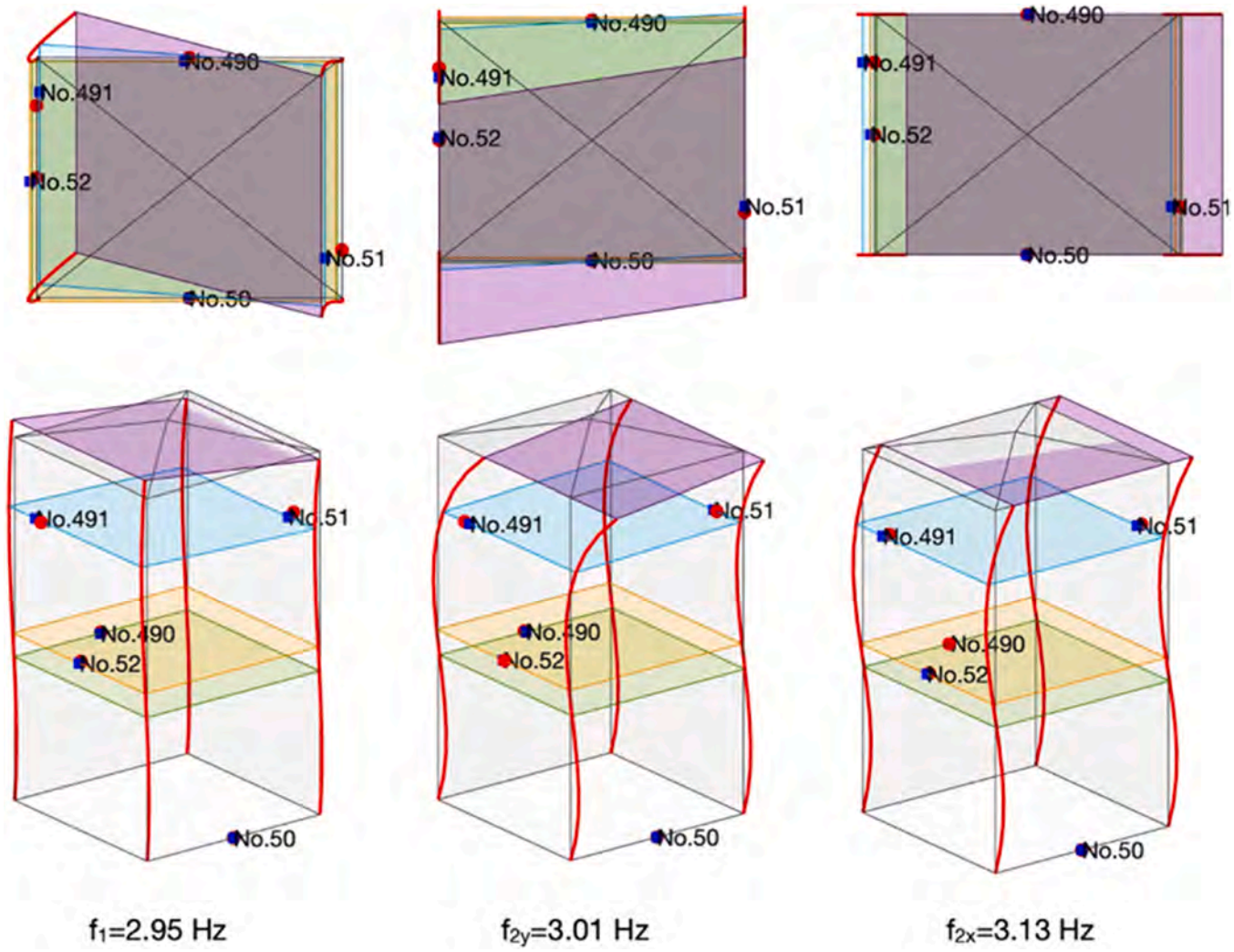

Fig. 25. Mode shapes of the Moletta tower.

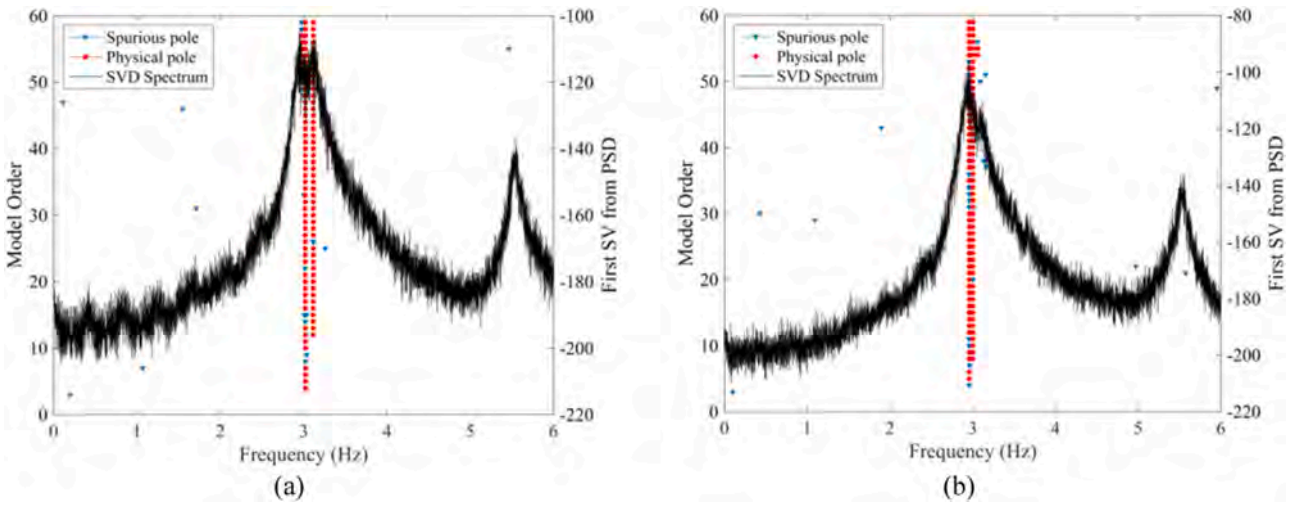

Fig. 26. Obtained stabilization diagrams. (a) *x*-direction, (b) *y*-direction.

Table 4
Comparison of the Moletta tower frequencies obtained through different methods.

Method	FDD, Puzzilli et al. (2021)		FDD (2023)		AFDD (2023)		Cov-SSI (2023)	
Direction	*x*	*y*	*x*	*y*	*x*	*y*	*x*	*y*
Identified	3.25	3.00	2.95	2.95	2.95	2.95	3.02	2.95
Frequencies	5.80	5.80	3.13	3.13	3.14	3.01	3.11	3
[Hz]	-		5.55	5.55	5.23	5.86	-	

Thus, anthropic vibrations could potentially be a source of damage. The Moletta tower is located on the south-east part of the Circus Maximus, as illustrated in Fig. 22. In this figure, the x and y axes denote the spatial reference system used to orient the SHM sensors. The structure has an irregular plan with varying wall sections and in 2013 it was retrofitted through steel rings and rods, stairs connected to the external walls, and reinforcement of the foundations. The tower was monitored using Wi-Fi tri-axial accelerometers located at various elevations (Fig. 23). The acceleration records were acquired on October 21, 2022, from 9:15 a.m. to 10:45 a.m. UTC. In the AFDD analysis, the frequency range is fixed between 0 and 6 Hz, and the number of required outputs is set to 3.

Fig. 24 illustrates the automatically selected frequencies in the SV spectrum. Three dynamic modes were identified in each of the two principal directions. It can be observed that some of the selected values do not correspond to clear peaks. In the traditional FDD analysis, the frequencies corresponding to the three main visible peaks would be chosen, i.e., $f_1 = 2.95$ Hz, $f_2 = 3.13$ Hz, $f_3 = 5.55$ Hz in both directions. On the other hand, the AFDD algorithm selected a slightly different second mode in the *y*-direction (3.01 Hz) and quite different third modes in both *x* and *y* directions (5.23 Hz and 5.86 Hz respectively). Slight differences in frequency estimation maybe due to the large number of points considered in the calculation of the SV spectrum. Further analysis revealed that the 5.55 Hz peak was filtered out because the MAC between this and the selected 3.14 Hz frequency was equal to 0.57 which exceeds the threshold of 0.2. In the *y*-direction, an analogous situation occurs. The third selected mode has a frequency equal to 5.86 Hz. The mode at 5.55 Hz is discarded because its MAC with the second identified mode (f=3.01 Hz) is 0.71. Fig. 25 illustrates the 3D mode shapes obtained from AFDD analysis. The top views highlight the rotation of the tower in the modes with frequencies 2.95 Hz and 3.01 Hz, which could be due to the stairs added in the 2013 retrofit interventions.

In the cov-SSI analysis, the order was set to 60 and the time lag to 125 based on Eq.12 [35,36]. The resulting stabilization diagrams in *x* and *y* directions are presented in Fig. 26, where it can be seen that only two stable modes were detected in each direction and that the cov-SSI algorithm failed at selecting a mode around the 5.55 Hz peak.

The extracted modal properties are summarized in Table 4 and compared to the study carried on by Puzzilli et al. [20]. Overall, a reduction in the frequency estimates can be noticed, which could indicate the dynamics of the structure might have changed. Despite the AFDD performed better than the cov-SSI, both methodologies delivered inconsistent results. Given the torsional behavior of the structure, a different sensor layout with two or more sensors on the same level could provide better results.

6. Conclusions

This research presented an optimized AFDD methodology based on MAC for modal identification to process SHM acceleration data. The optimization process involved a series of sensitivity analyses to determine the optimal MAC threshold. The influence of noise levels, record length, and SHM spatial resolution was explored using the Yonge cable-stayed bridge as case study. Stabilization diagrams were generated using the results obtained from the AFDD and FE target values. Through sensitivity analyses, GMM was applied to obtain a robust range for the MAC threshold, reducing the need for expert intervention and preliminary studies. The first outcome of this research is that a MAC threshold of 0.2 consistently led to optimal results.

The proposed methodology was tested on three case studies, namely the Yonghe cable-stayed bridge, the PolyU footbridge, and the Moletta tower. This approach allowed to evaluate its robustness and limitations when applied to structures with significantly different dynamics, which would not be evident considering only a single case study.

The conclusions that can be made from the analysis of each case study are the following.

- In the analysis of the Yonghe cable-stayed bridge, the clear differences in the vertical modes made the modal identification task relatively easy. The AFDD showed better performance in detecting the actual modal properties and handling spurious modes compared to cov-SSI.
- In the modal identification of the PolyU footbridge, the AFDD procedure could accurately identify frequencies but struggled to detect a complex torsional mode. This limitation is due to the fact that the AFDD relies on the geometry of mode shapes, and the torsional mode was filtered out because similar other modes.
- The Moletta tower, was selected as an example of cultural heritage structure with large uncertainties in material properties,

construction techniques, ageing, damage, effect of retrofit interventions. The optimized AFDD performed better than the cov-SSI and successfully identified changes in the dynamic performance of the Moletta tower over time. This can be viewed as an indication of damage or stiffness reduction. Therefore, the method could be a valuable tool for long-term monitoring of heritage structures. However, since mode shapes are low sensitivity structural properties, it is recommended to thoroughly verify the accuracy of the actual shape by adopting a proper sensor layout.

Overall, from the application of the method to multiple case studies, the following conclusions can be made:

- The $\alpha = 0.2$ threshold was effective in all three case studies, suggesting that it can be applied to a wide spectrum of structures.
- The AFDD outperforms cov-SSI in estimating vertical and transversal modes, and overcomes the challenging task of interpreting ambiguous stabilization diagrams.
- The method may struggle to identify modes with complex geometries and to distinguish between modes with similar geometries, for which it is recommended to use a sensor layout with higher spatial resolution.
- The method could be beneficial for researchers and professional engineers to help owners and managers developing strategic plans for early damage detection and optimal maintenance, extending the operational lifespan of critical and cultural heritage structures.

In conclusion, it is observed that finding an approach that could be applied consistently and invariably, i.e., without having to calibrate any parameters, remains still a challenge. Existing automated OMA procedures may work flawlessly for simple structures, but in complex cases it could be necessary to re-define some calibration parameters. The proposed procedure is intended as a practical tool that considers different crucial variables to optimize the selection of the MAC threshold. While this approach represents a step forward, it is worth noting that further research is needed to reach a full automation of OMA using SHM data. The development of new algorithms and applications to a vast range of substantially different structures could help in achieving the objective of a fully automated data-driven procedure.

CRediT authorship contribution statement

Alessandro Cardoni: Writing – review & editing, Writing – original draft, Visualization, Methodology, Data curation, Conceptualization. **Amir Reza Elahi:** Writing – original draft, Visualization, Methodology, Formal analysis, Conceptualization. **Gian Paolo Cimellaro:** Writing – review & editing, Project administration, Methodology, Data curation.

Declaration of Competing Interest

The authors declare that they have no known competing financial interests or personal relationships that could have appeared to influence the work reported in this paper.

Acknowledgements

The authors would like to thank: Prof. Li Shunlong from the Harbin Institute of Technology (China) for providing us with the FE model of the Yonghe cable stayed-bridge; Prof. Yong XIA from the Hong Kong Polytechnic University for providing us with data related to the PolyU footbridge; the Capitoline Superintendence of Rome for their support during the Moletta tower monitoring campaigns; Mauro Spampani and Alessandro Mitillo from Lunitek S.r.l (Italy) for providing the SHM sensors and their support in the data collection of the Moletta tower monitoring campaigns.

Data Availability

Data will be made available on request.

References

[1] Tronci EM, De Angelis M, Betti R, Altomare V. Vibration-based structural health monitoring of a RC-masonry tower equipped with non-conventional TMD. Eng Struct Dec. 2020;224:111212. https://doi.org/10.1016/j.engstruct.2020.111212.
[2] Petersen ØW, Øiseth O. Sensitivity-based finite element model updating of a pontoon bridge. Eng Struct Nov. 2017;150:573–84. https://doi.org/10.1016/j.engstruct.2017.07.025.
[3] Torres W, Almazán JL, Sandoval C, Boroschek R. Operational modal analysis and FE model updating of the Metropolitan Cathedral of Santiago, Chile. Eng Struct Jul. 2017;143:169–88. https://doi.org/10.1016/j.engstruct.2017.04.008.
[4] Scozzese F, Ragni L, Tubaldi E, Gara F. Modal properties variation and collapse assessment of masonry arch bridges under scour action. Eng Struct Nov. 2019;199:109665. https://doi.org/10.1016/j.engstruct.2019.109665.
[5] García-Macías E, Ubertini F. Automated operational modal analysis and ambient noise deconvolution interferometry for the full structural identification of historic towers: A case study of the Sciri Tower in Perugia, Italy. Eng Struct Jul. 2020;215:110615. https://doi.org/10.1016/j.engstruct.2020.110615.
[6] Zhou X, Kim C-W, Zhang F-L, Chang K-C. Vibration-based Bayesian model updating of an actual steel truss bridge subjected to incremental damage. Eng Struct Jun. 2022;260:114226. https://doi.org/10.1016/j.engstruct.2022.114226.
[7] Pereira S, Magalhães F, Gomes JP, Cunha Á, Lemos JV. Vibration-based damage detection of a concrete arch dam. Eng Struct May 2021;235:112032. https://doi.org/10.1016/j.engstruct.2021.112032.
[8] Cardoni A, Cimellaro GP. The role of reinforced concrete roofs in the seismic performance of masonry buildings. J Build Eng Mar. 2020;28:101056. https://doi.org/10.1016/j.jobe.2019.101056.
[9] Pellecchia C, Cardoni A, Cimellaro GP, Domaneschi M, Ansari F, Khalil AA. Progressive collapse analysis of the champlain towers south in surfside, Florida. J Struct Eng Jan. 2024;150(1):04023211. https://doi.org/10.1061/JSENDH.STENG-12485.
[10] Aghabeigi P, Farahmand-Tabar S. Seismic vulnerability assessment and retrofitting of historic masonry building of Malek Timche in Tabriz Grand Bazaar. Eng Struct Aug. 2021;240:112418. https://doi.org/10.1016/j.engstruct.2021.112418.
[11] Van Overschee P, De Moor B. Subspace Identif Linear Syst 1996. https://doi.org/10.1007/978-1-4613-0465-4_6.
[12] S. Kumar, "Statistical system identification of structures using ARMA models", 1993, Accessed: Nov. 08, 2023. [Online]. Available: ⟨https://hdl.handle.net/1911/13750⟩.
[13] Bertha M, Golinval J-C. Identification of non-stationary dynamical systems using multivariate ARMA models. Mech Syst Signal Process May 2017;88:166–79. https://doi.org/10.1016/j.ymssp.2016.11.024.
[14] Boroschek RL, Bilbao JA. Interpretation of stabilization diagrams using density-based clustering algorithm. Eng Struct Jan. 2019;178:245–57. https://doi.org/10.1016/j.engstruct.2018.09.091.
[15] B. Peeters, G. De Roeck, L. Hermans, T. Wauters, C. Krmer, and C. Smet, "Comparison of System Identification Methods Using Operational Data of a Bridge Test", May 2000.
[16] Brincker R, Zhang L, Andersen P. Modal identification of output-only systems using frequency domain decomposition. Smart Mater Struct Jun. 2001;10(3):441–5. https://doi.org/10.1088/0964-1726/10/3/303.
[17] Brincker R, Ventura C, Andersen P. Damping estimation by frequency domain decomposition. Proc Int Modal Anal Conf - IMAC Jan. 2001.
[18] An Y, Chatzi E, Sim S, Laflamme S, Blachowski B, Ou J. Recent progress and future trends on damage identification methods for bridge structures. Struct Control Health Monit Oct. 2019;26(10). https://doi.org/10.1002/stc.2416.
[19] Xia Q, et al. System design and demonstration of performance monitoring of a butterfly-shaped arch footbridge. Struct Control Health Monit Jul. 2021;28(7). https://doi.org/10.1002/stc.2738.
[20] Puzzilli LM, Bongiovanni G, Clemente P, Di Fiore V, Verrubbi V. Effects of anthropic and ambient vibrations on archaeological sites: the case of the circus maximus in Rome. Geosciences Nov. 2021;11(11):463. https://doi.org/10.3390/geosciences11110463.
[21] Li J, Bao T, Ventura CE. A robust methodology for output-only modal identification of civil engineering structures. Eng Struct Nov. 2022;270:114764. https://doi.org/10.1016/j.engstruct.2022.114764.
[22] Zhong Q-M, Chen S-Z, Sun Z, Tian L-C. Fully automatic operational modal analysis method based on statistical rule enhanced adaptive clustering method. Eng Struct Jan. 2023;274:115216. https://doi.org/10.1016/j.engstruct.2022.115216.
[23] Magalhães F, Cunha Á, Caetano E. Online automatic identification of the modal parameters of a long span arch bridge. Mech Syst Signal Process Feb. 2009;23(2):316–29. https://doi.org/10.1016/j.ymssp.2008.05.003.
[24] Zini G, Betti M, Bartoli G. A quality-based automated procedure for operational modal analysis. Mech Syst Signal Process Feb. 2022;164:108173. https://doi.org/10.1016/j.ymssp.2021.108173.
[25] Romanazzi A, Scocciolini D, Savoia M, Buratti N. Iterative hierarchical clustering algorithm for automated operational modal analysis. Autom Constr Dec. 2023;156:105137. https://doi.org/10.1016/j.autcon.2023.105137.

[26] Rosso MM, Aloisio A, Parol J, Marano GC, Quaranta G. Intelligent automatic operational modal analysis. Mech Syst Signal Process Oct. 2023;201:110669. https://doi.org/10.1016/j.ymssp.2023.110669.
[27] Ye X, Huang P, Pan C, Mei L. "Innovative stabilization diagram for automated structural modal identification based on ERA and hierarchical cluster analysis". J Civ Struct Health Monit Nov. 2021;11(5):1355–73. https://doi.org/10.1007/s13349-021-00514-8.
[28] James G, Carne T, Laufer J. The natural excitation technique (NExT) for modal parameter extraction from operating structures. J Anal Exp Modal Anal Jan. 1995;10.
[29] Dederichs AC, Øiseth O. Experimental comparison of automatic operational modal analysis algorithms for application to long-span road bridges. Mech Syst Signal Process Sep. 2023;199:110485. https://doi.org/10.1016/j.ymssp.2023.110485.
[30] Sun Q, Rainieri C, Ren WX, Yan WJ, Fabbrocino G. Automated operational modal analysis of bell towers subjected to narrowband input. Structures Aug. 2023;54:78–88. https://doi.org/10.1016/j.istruc.2023.05.034.
[31] Kim H, Sim S. Automated peak picking using region-based convolutional neural network for operational modal analysis. Struct Control Health Monit Nov. 2019;26(11). https://doi.org/10.1002/stc.2436.
[32] Jeong S, Kim H, Lee J, Sim S-H. Automated wireless monitoring system for cable tension forces using deep learning. Struct Health Monit Jul. 2021;20(4):1805–21. https://doi.org/10.1177/1475921720935837.
[33] Brincker R, Andersen P, Jacobsen N-J. Automated frequency domain decomposition for operational modal analysis. IMAC-XXIV Conf Expo Struct Dyn Jan. 2007.
[34] Magalhães F, Cunha Á, Caetano E. Dynamic monitoring of a long span arch bridge. Eng Struct Nov. 2008;30(11):3034–44. https://doi.org/10.1016/j.engstruct.2008.04.020.
[35] Bishop CM. *Pattern recognition and machine learning*, 13. (corrected at 8th printing 2009). in Information science and statistics. New York: Springer,; 2009.
[36] Reynolds DA, Rose RC. Robust text-independent speaker identification using Gaussian mixture speaker models. IEEE Trans Speech Audio Process Jan. 1995;3(1):72–83. https://doi.org/10.1109/89.365379.
[37] Dempster AP, Laird NM, Rubin DB. Maximum likelihood from incomplete data via the *EM* algorithm. J R Stat Soc Ser B Methodol Sep. 1977;39(1):1–22. https://doi.org/10.1111/j.2517-6161.1977.tb01600.x.
[38] Hermans L, Van Der Auweraer H. Modal testing and analysis of structures under operational conditions: industrial applications. Mech Syst Signal Process Mar. 1999;13(2):193–216. https://doi.org/10.1006/mssp.1998.1211.
[39] Zhou K, Li Q-S, Han X-L. Modal identification of civil structures via stochastic subspace algorithm with monte carlo–based stabilization diagram. J Struct Eng Jun. 2022;148(6):04022066. https://doi.org/10.1061/(ASCE)ST.1943-541X.0003353.
[40] Wu Wen-Hwa, Wang Sheng-Wei, Chen Chien-Chou, Lai Gwolong. Mode identifiability of a cable-stayed bridge under different excitation conditions assessed with an improved algorithm based on stochastic subspace identification. Smart Struct Syst Mar. 2016;17(3):363–89. https://doi.org/10.12989/SSS.2016.17.3.363.
[41] Lee S-Y, Huynh T-C, Kim J-T. A practical scheme of vibration monitoring and modal analysis for caisson breakwater. Coast Eng Jul. 2018;137:103–19. https://doi.org/10.1016/j.coastaleng.2018.03.008.
[42] A. Otto, "OoMA Toolbox." Accessed: Nov. 06, 2023. [Online]. Available: (⟨https://www.mathworks.com/matlabcentral/fileexchange/68657-ooma-toolbox⟩), MATLAB Central File Exchange. Retrieved December 2, 2022.
[43] Li S, Li H, Liu Y, Lan C, Zhou W, Ou J. "SMC structural health monitoring benchmark problem using monitored data from an actual cable-stayed bridge: SMC Structural Health Monitoring Benchmark Problem". Struct Control Health Monit Feb. 2014;21(2):156–72. https://doi.org/10.1002/stc.1559.
[44] "Ansys Mechanical APDL,." Accessed: Nov. 06, 2023. [Online]. Available: ⟨https://www.ansys.com⟩.
[45] García-Macías E, Ubertini F. Structural assessment of bridges through ambient noise deconvolution interferometry: application to the lateral dynamic behaviour of a RC multi-span viaduct. Arch Civ Mech Eng Aug. 2021;21(3):123. https://doi.org/10.1007/s43452-021-00273-9.
[46] Papazafeiropoulos G, Plevris V. Openseismomatlab: a new open-source software for strong ground motion data processing. Heliyon Sep. 2018;4(9):e00784. https://doi.org/10.1016/j.heliyon.2018.e00784.
[47] Sanliturk KY, Cakar O. Noise elimination from measured frequency response functions. Mech Syst Signal Process May 2005;19(3):615–31. https://doi.org/10.1016/j.ymssp.2004.04.005.
[48] Ravizza G, Ferrari R, Rizzi E, Dertimanis V. On the denoising of structural vibration response records from low-cost sensors: a critical comparison and assessment. J Civ Struct Health Monit Nov. 2021;11(5):1201–24. https://doi.org/10.1007/s13349-021-00502-y.
[49] R. Cantieni, "Experimental methods used in system identification of civil engineering structures", in *Proceedings of the International Operational Modal Analysis Conference (IOMAC)*, Citeseer, 2005, pp. 249–260. Accessed: Sep. 26, 2024. [Online]. Available: ⟨https://citeseerx.ist.psu.edu/document?repid=rep1&type=pdf&doi=5e3ab207814946a98afea93296c8950c4da55321⟩.
[50] Pereira S, Magalhães F, Cunha Á, Moutinho C, Pacheco J. Modal identification of concrete dams under natural excitation. J Civ Struct Health Monit Apr. 2021;11(2):465–84. https://doi.org/10.1007/s13349-020-00462-9.
[51] Brincker R, Ventura C. Introduction to Operational Modal Analysis. John Wiley & Sons, Ltd; 2015. https://doi.org/10.1002/9781118535141.